Sunlight driven photocatalytic degradation of RhB dye using composite of bismuth oxy-bromide kaolinite BiOBr@Kaol: Experimental and molecular dynamic simulation studies

Hamza Ighnih, Redouane Haounati, Rahime Eshaghi Malekshah, Hassan Ouachtak, Yahya Toubi, Fadi Alakhras, Amane Jada, Abdelaziz Ait Addi

Sunlight driven photocatalytic degradation of RhB dye using composite of bismuth oxy-bromide kaolinite BiOBr@Kaol: Experimental and molecular dynamic simulation studies

Hamza Ighnih[1,*], Redouane Haounati[1], Rahime Eshaghi Malekshah[2], Hassan Ouachtak[1, 3, *], Yahya Toubi [1, 3], Fadi Alakhras[4], Amane Jada[5,6, *], Abdelaziz Ait Addi[1, *]

[1] Laboratory of Organic and Physical Chemistry, Faculty of Science, Ibn Zohr University, Agadir, Morocco

[2] Department of Chemistry, Faculty of Chemistry, University of Semnan, Semnan, Iran

[3] Faculty of Applied Science, Ait Melloul, Ibn Zohr University, Agadir, Morocco

[4] College of Pharmacy, Middle East University, Amman, 11831, Jordan

[5] Institute of Materials Science of Mulhouse (IS2M), Haute Alsace University, Mulhouse 68100, France

[6] Strasbourg University, Strasbourg 67081, France

*Corresponding authors:

ouachtakhassan@gmail.com; hamza.ighnih@edu.uiz.ac.ma;

amane.jada@uha.fr ; a.aitaddi@uiz.ac.ma

Graphical abstract

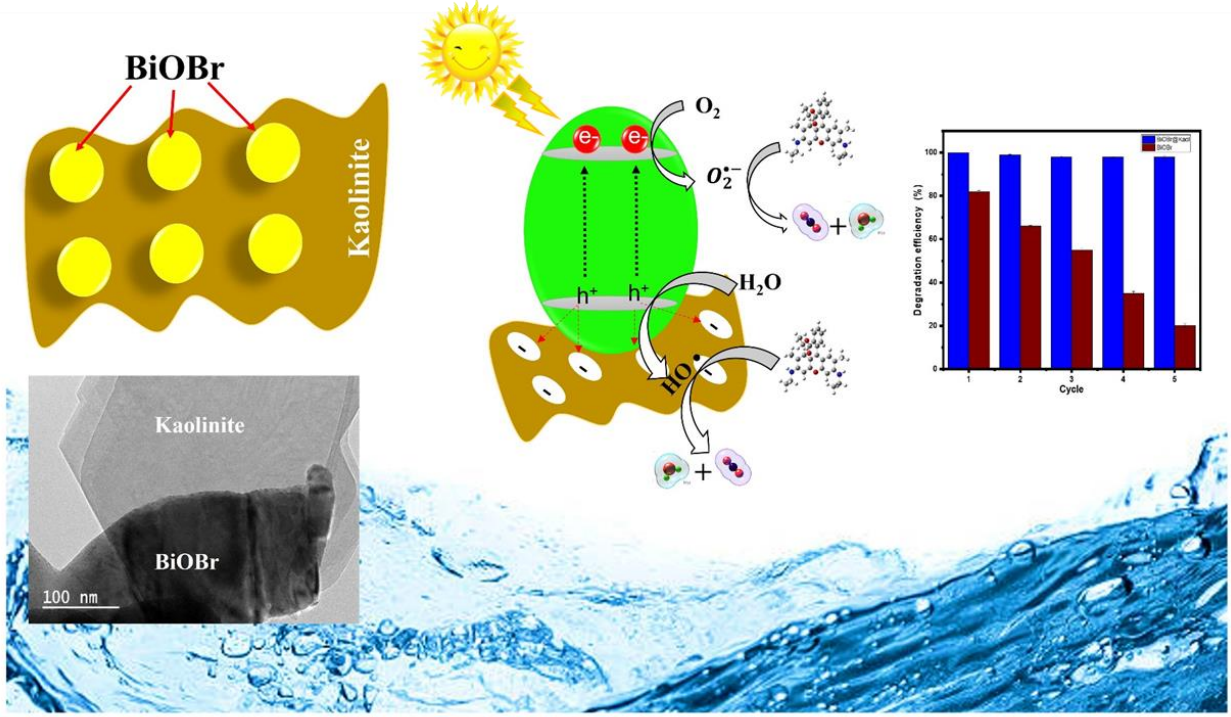

Highlights

- **BiOBr@Kaol** nanocomposite photocatalysts were synthesized by co-precipitation method.
- The **BiOBr@Kaol** nanocomposites were effective for photodegradation of RhB toxic dye under sunlight irradiation.
- The best degradation performance (~100%) was obtained by **BiOBr@0.4Kaol** nanocomposite.
- A prospective mechanism of RhB degradation by **BiOBr@0.4Kaol** nanocomposite was designed.

Abstract

This study reported the synthesis of a new eco-friendly photocatalyst nanocomposite based on kaolinite clay and bismuth oxybromide (BiOBr@Kaolinite) using a facile co-precipitation method in acidic medium. The prepared nanocomposite was characterized using several techniques such as X-ray diffraction (XRD), Fourier transform infrared spectroscopy (FTIR), scanning microscopy electron (SEM), Transmission electron microscope (TEM), Energy-dispersive X-ray spectroscopy (EDX), UV–Vis diffuse reflectance spectra (DRS), and X-ray photoelectron spectroscopy (XPS). These techniques were used to determine the crystal phase, functional groups, morphology, elementary composition, chemical states, optical properties, and bad gap energy of as synthesized, respectively. The characterized materials were then applied for rapid photodegradation of Rhodamine B dye (RhB), indicating its effective use for the degradation of toxic organic pollutants under sunlight irradiation. The photocatalytic activity study showed that RhB dye (10 mg/L) was degraded within 30 minutes under sunlight irradiation. The degradation mechanism of RhB and the photocatalytic stability study of the nanocomposite BiOBr@0.4Kaol showed that, the high photocatalytic activity could be attributed to the charge transfer from kaolinite to BiOBr nanoparticles, which prevented the rapid recombination of the electron-hole pair induced during the photocatalytic process. Moreover, MD and DFT-D stimulations and adsorption calculations based on Monte Carlo were applied in this study. This study led to the development of an effective and environmentally friendly photocatalyst nanocomposite for the degradation of toxic organic pollutants in wastewater, highlighting its potential application in water treatment and depollution processes.

Keywords: Kaolinite, BiOBr, Co-precipitation, RhB dye, photocatalysis, sunlight, theoretical calculations.

1. Introduction

Nowadays, with the rapid increase of the industrial sector, the volume of wastewater generated by this sector is strongly increasing [1,2]. Wastewater from sewage plants often contains toxic organic compounds that are difficult to biodegrade [3]. Among these organic compounds, the Rhodamine B dye (RhB) has garnered attention due to its hazardous effects [4,5]. RhB is highly toxic, carcinogenic, and possesses a stable molecular structure in aqueous media, which makes it resistant to biodegradation and poses a significant threat to human health and the environment [6,7].

The use of reliable and sustainable treatment methods for the industrial wastewater should be necessary to achieve depollution and facilitate the reuse of purified water [8–10]. Various techniques, such as adsorption [11], coagulation-flocculation [12], and membrane technology [13], have been employed to remove toxic organic compounds. However, these methods primarily concentrate the pollutants on a substrate without breaking down the organic molecules. In contrast, advanced oxidation processes (AOPs) have gained significant attention from researchers worldwide due to their cost-effectiveness, practical applicability, ease of use, and high efficiency in water mineralization [14–16]. Heterogeneous photocatalysis has emerged as one of the most effective advanced oxidation processes (AOPs) for wastewater treatment and complete degradation of organic pollutants, particularly dyes [17]. This technology is based on the principle of exciting a semiconductor material using an artificial or natural radiation source [18]. Upon excitation, the semiconductor generates electron-hole pairs (e- and h+), which in turn generate reactive species such as hydroxyl radicals ($^{\bullet}HO$) and superoxide radicals ($^{\bullet}O_2^-$) [19]. These radicals play a crucial role in the photodegradation of pollutants, converting them into harmless products such as water (H_2O) and carbon dioxide (CO_2).

Recently, various semiconductors (photocatalysts) have been utilized in the photodegradation process for removing toxic organic compounds, including g-C_3N_4 [20], Ag/AgBr [21], Ag_2O [17], ZnO [22], TiO_2 [23]. Hence, these photocatalysts have several drawbacks that limit their application, such as, high cost, electron-hole recombination, lower efficiency, and difficulties in regeneration [24]. Bismuth-based semiconductors [25] such as $BiPO_4$ [26], $BiVO_4$, Bi_2WO_6, Bi_2MoO_6 [27], $BiFeO_3$ [28], $Bi_4Ti_3O_{12}$ [29], as well as BiOBr have been synthesized and utilized in photocatalytic applications. Among them, BiOBr semiconductor has gained significant attention due to its stability, non-toxicity, corrosion resistance, superior electrical conductivity, unique structure (**Fig. 1-a**), good photocatalytic performance, and suitable band

gap for various applications [30–33]. However, pure BiOBr photocatalyst suffers from issues such as agglomeration in solution, low photo-generated charge separation, lengthy treatment time, and limited photocatalytic power under sunlight, which have hindered its practical applications [3]. To address these challenges, several studies have made significant efforts to enhance the performance of pure BiOBr by forming heterojunctions with other photocatalytic semiconductors, such as BiOBr/TiO_2 [25], ZnO/BiOBr [34], BiOBr/g-C_3N_4 [35]. However, these solutions are cost-intensive and not applicable under sunlight. A potential solution to improve the photocatalytic performance is the utilization of pure BiOBr catalysts under solar light irradiation with the aid of natural clay minerals [36], including montmorillonite [37], sepiolite [38], have been employed to address issues such as easy agglomeration and electron-hole pair recombination in BiOBr semiconductors. However, the use of kaolinite clay as a carrier for BiOBr semiconductor shows the enhancement photocatalytic performance under sunlight irradiation due to the higher surface area allows for increased adsorption, the interface promotes efficient charge transfer and separation of photogenerated electron-hole pairs, the stability and reusability of the photocatalyst [39,40].

In this study, BiOBr@Kaolinite nanocomposite photocatalysts were successfully synthesized using a facile co-precipitation method in an acidic medium. The synthesized nanocomposites were characterized using various techniques. X-ray diffraction (XRD) was employed to study the structures, Fourier-transform infrared spectroscopy (FT-IR) was performed to determine the crystal phase, Scanning Electron Microscopy (SEM) was used to observe the topography, Transmission Electron Microscopy (TEM) was utilized to visualize the morphologies and nanostructures, X-ray photoelectron spectroscopy (XPS) was used to identify chemical species at the surface, UV-vis Diffuse Reflectance Spectroscopy (DRS) to study the optical properties and bang gape energy. The characterized samples were then tested for their ability to degrade the hazardous RhB dye in an aqueous solution under sunlight irradiation. Additionally, molecular dynamics (MD) and Density Functional Theory with dispersion correction (DFT-D) simulations, as well as adsorption calculations based on Monte Carlo, were applied in this study.

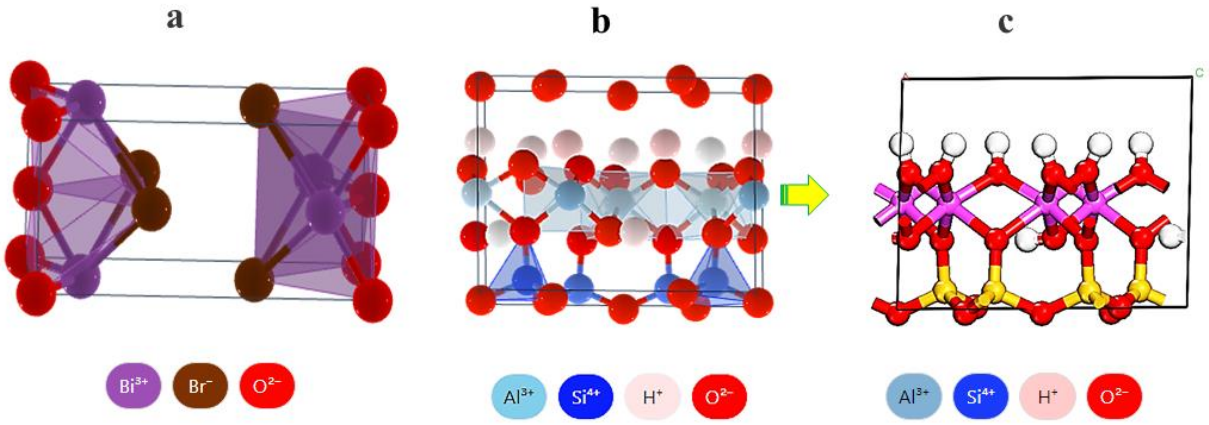

Figure 1: The side view of BiOBr crystals unit cells, and (b and c) views of kaolinite clay unit cells.

2. Material and methods

2.1. Photocatalysts preparation

2.1.1. Materials and reagents

The natural kaolinite clay, the bismuth nitrate pentahydrate extra-pure, the glacial acetic acid ($CH_3CO_2H \geq 99.95\%$) and rhodamine B (RhB) used in this study were purchased from Sigma–Aldrich, while sodium bromide ($NaBr \geq 99.5\%$) was obtained from Scharlau. All these chemical reagents were applied without any further purification.

2.1.2. Preparation of BiOBr and BiOBr@Kaol

The BiOBr@Kaol was prepared using the co-precipitation method in an acidic medium. Firstly, 3.3 mmol of bismuth nitrate pentahydrate extra-pure was dissolved completely in 40 mL of glacial acetic acid/ deionized water (1:1) solution at 25 °C for 1 h to obtain a transparency liquid. After that, 1 g of kaolinite clay was added to the solution and stirred for 1 hour (Solution A). Another solution of sodium bromide was prepared by dissolving of 3.3 mmol of NaBr in 30 mL of deionized water under vigorous stirring for 30 min (solution B). Then, solution B was slowly added to solution A under vigorous stirring for 5 h. Finally, the precipitate was filtered, washed three times with distilled water and ethanol, and dried at 70 °C for 12 h and signed BiOBr@1.0Kaol. According to this procedure, BiOBr@Kaol composites with a different mass of kaolinite (0.2, 0.4, 0.6, and 0.8 g) were synthesized and named as BiOBr@0.2Kaol, BiOBr@0.4Kaol, BiOBr@0.6Kaol, and BiOBr@0.8Kaol, respectively. The same way was applied for the synthesis of a pure BiOBr without adding

kaolinite. **Figure.2** shows a brief summary of the steps involved in the preparation of the BiOBr@Kaol nanocomposite.

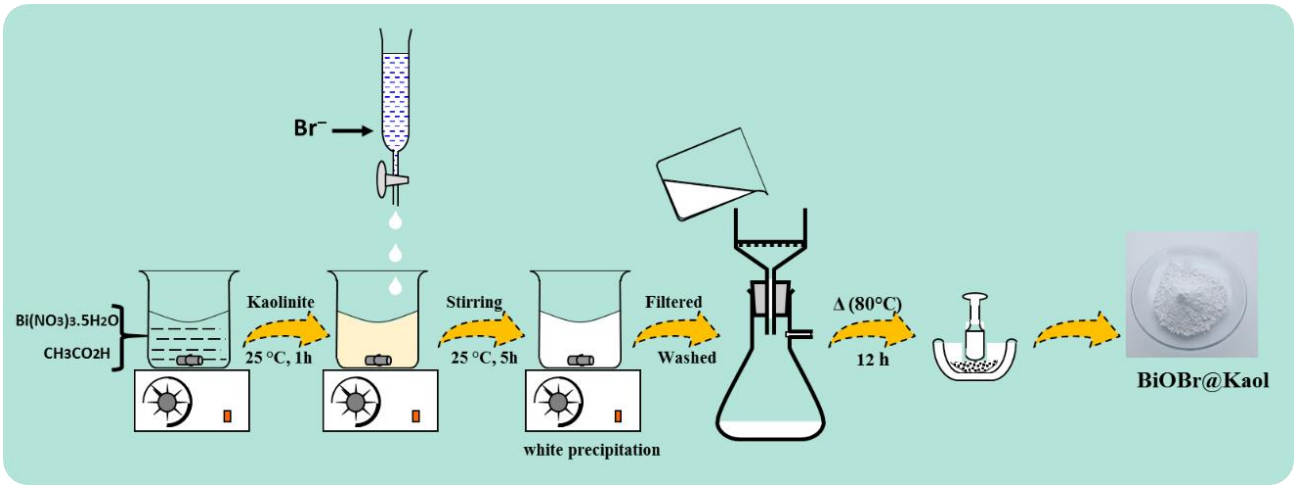

Figure 2: Strategies of the synthesis of the BiOBr@Kaol photocatalysts.

2.2. Samples characterization

The phase and crystallinity of the kaolinite and the prepared photocatalysts were investigated using X-ray diffraction (Bruker D8 Twin) with monochromatic λ(KαCu) = 1.5418 Å radiation at a step size of 0.05° and a scan rate of 1 s/step. The functional groups were analyzed in the wavenumber region from 400 to 4000 cm^{-1} using Fourier Transform Infrared Spectroscopy (Shimadzu spectrometer equipped with a Jasco ATR PRO ONE). The morphology and microstructure were analyzed by scanning electron microscopy (Supra 40 VP Gemini Zeiss Column, with a maximum voltage of 20 kV), and the elemental compositions of the nanocomposite were determined by recording their Energy Dispersive X-ray (EDX) spectra. The high resolution of the catalysts was analyzed by transmission electron microscopy (TEM). The chemical compositions and electronic states were characterized using X-ray photoelectron spectroscopy (XPS). The band gap of the as-synthesized catalysts was measured using UV-Vis diffuse reflectance spectra with a Lambda de PerkinElmer instrument.

2.3. Photocatalysis processes

The photocatalytic degradation of RhB dye in aqueous solution over as-prepared nanocomposites was investigated under sunlight irradiation that performed in the month of April 2022 between 11:40 A.M. and 12:40 P.M. 100 mL of RhB dye (10 mg/L) solutions were mixed in a reactor with 100 mg of the photocatalyst. Prior to sunlight irradiation, the reactor was maintained in the dark for one hour until an adsorption-desorption equilibrium was established between RhB dye and the photocatalyst. Under the sunlight irradiation, 4 mL

of the solution was collected each 5 min, centrifuged, and the concentration of residual RhB dye was measured using a UV spectrometer (UV- 1800, SHIMADZU), at the wavelength of 554 nm. The degradation efficiency (%) and the rate constants K (min^{-1}) are calculated using **Equations 1** and **2**, respectively:

$$DE\% = \frac{C_0 - C_t}{C_0} \times 100 \quad (1)$$

$$Ln\left(\frac{C_0}{C_t}\right) = K \times t \quad (2)$$

Herein, C_0 and C_t are the concentrations of the RhB dye at the initial and any time during photodegradation, respectively. K (min^{-1}) is the constant of the first-order reaction.

2.4. Calculation methods

2.4.1. Model Construction

Kaolinite (Kaol) as layered clay mineral containing of tetrahedral SiO_4 and octahedral AlO_6 periodically is shown in **Figure 3a** and **3b**. $Al_2Si_2H_4O_9$ (code; mp-695878) with Space Group; P1, *a* =5.21, *b* =7.48, *c* = 9.05 Å, α=91.79, β =89.73 γ = 104.97 ° and Volume= 340.74 $Å^3$ was downloaded from https://materialsproject.org/materials/mp-695878. Then, the crystal structure of Kaol (0 0 1) was designed on (0 0 1) surface and characterizations including thickness of 2.06 Å, set u v; 2 1, vacuum thickness (0.000) and slab position (1.00) **Figure 3 (c, d)**. **Figures (3-e and 3-f)** are showed designed Kaolinite surface without unit cell to optimize and adsorb BiOBr and pollutants which the structure of Kaolinite are included both two sides; Al-bterminated and Si-terminated surfaces [41]. BiOBr including (code; mp-23072) with Space Group; P4/nmm, Lattice System; Tetragonal *a* = *b* =3.93, c = 8.39 Å, α= β = γ = 90.000° and Volume= 129.51 $Å^3$ **Figures 3g** and **3h,** was downloaded from https://materialsproject.org/materials/mp-23072. BiOBr along the (001) facet was first studied [42]. In order to adsorb BiBr adsorption on Kaolinite, the crystal model was prepared from download primitive BiOBr cell with the structure of Bi-, O- and Br-terminated. So, this model was constructed in the (U V; 2 × 2) supercells (illustrated in **Figures (3-g and 3-h)**. at last, the optimized lattice parameters were obtained *a* = 8.394, *b* = 5.554, *c* = 5.554 Å, α= β = γ = 90.000°. BiOBr without cell box was applied for adsorption as observed in **Figures (3-k and 3-l)**.

Computational method

The electronic structures of typical Kaol, BiOBr and RhB were simulated using DFT-D method implementing $DMol^3$ in Materials Studio 2017. The electron exchange–correlation

energy of compunds was carried out by the generalized gradient approximation (GGA) developed by Perdew-Burke-Ernzerhof (PBE) in addition to the DFT-D correction. After optimization, to obtain the optimal adsorption sites and directions of BiOBr on Kaol (0 0 1) and RhB on BiOBr@Kaol surfaces, Monte Carlo simulations were performed with universal force field that the number of cycles and the van der Waals interactions were calculated under 10 cycles and the Group-based option at a cutoff of 12.5 Å. The hydroxyl groups of Al-terminated for the (0 0 1) surface and oxygen and silicon atoms for the (0 0 $\bar{1}$) surface of Kaolinite were free [43].

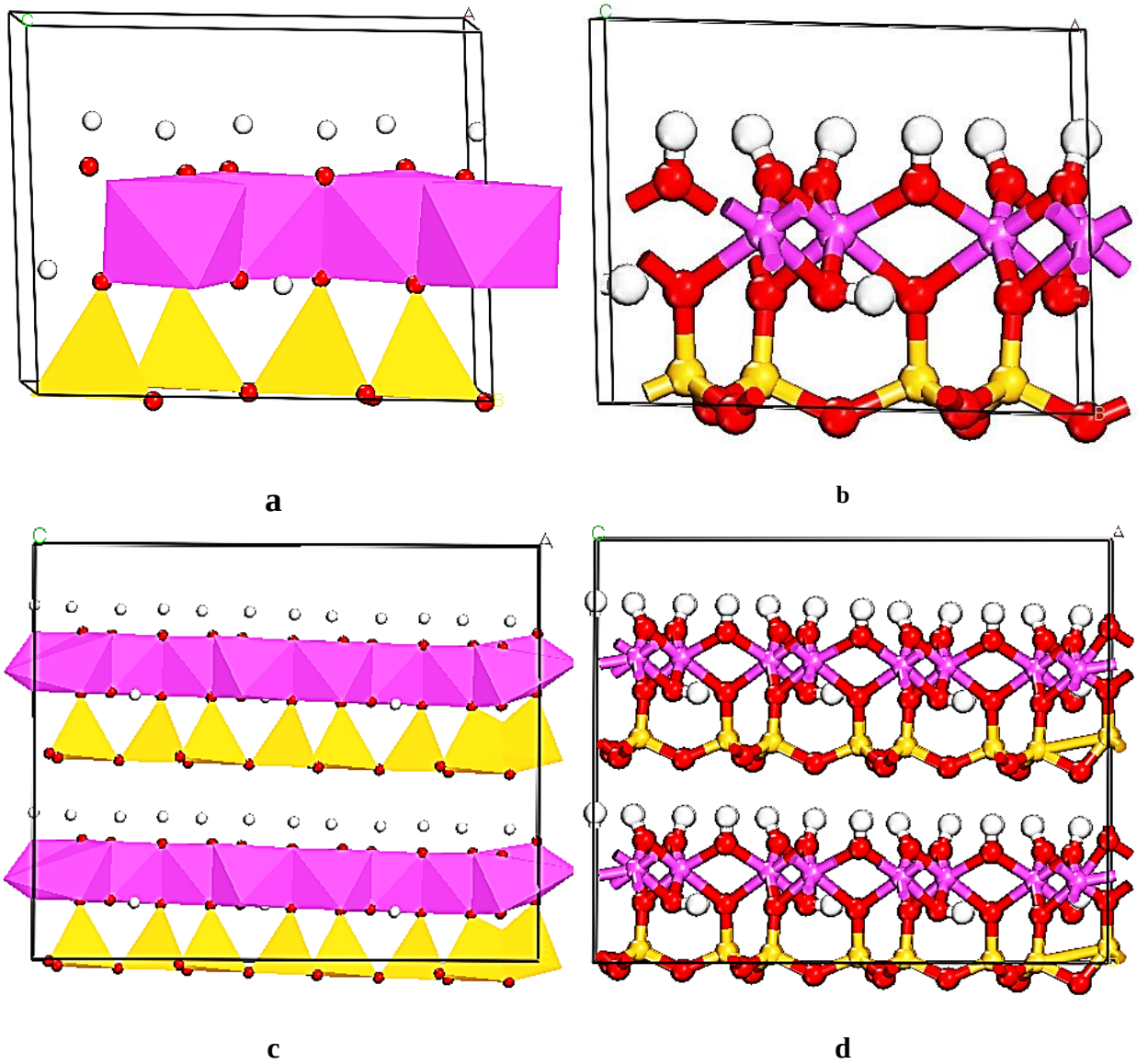

a **b**

c **d**

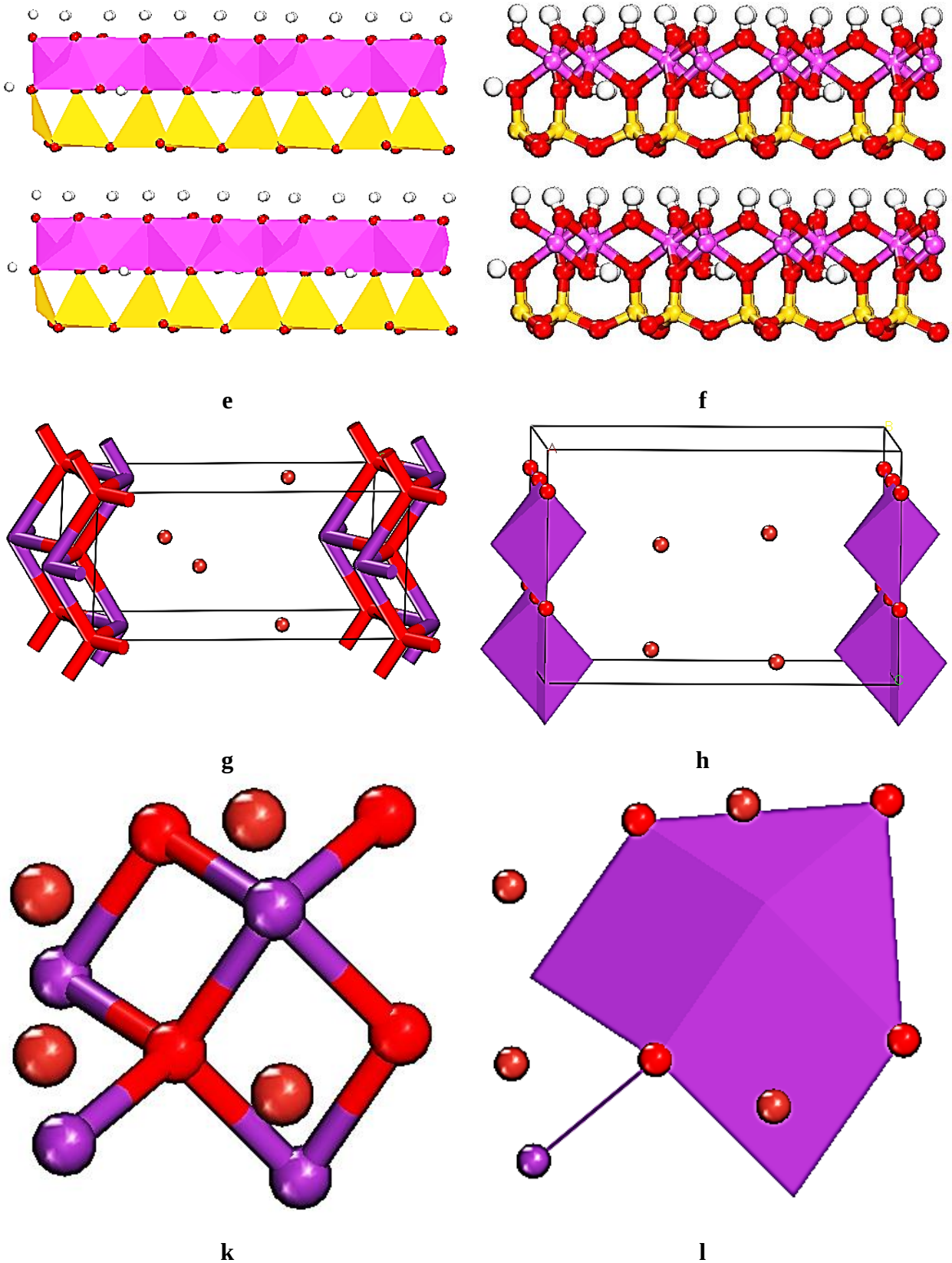

Figure 3: Snapshots of the proposed structures (a and b); $Al_2Si_2H_4O_9$ $(Kaol)_9$ (side), (c and d); side view of Kaol unit cell (0 0 1, U V; 2 1), (e and f); side view of Kaol without unit cell (001) (g and h); BiOBr unit cell, (g and h); BiOBr unit cell ((0 0 1), and thickness; 2.50), (k); BiOBr without unit cell (0 0 1). (The Si, Al, Br, Bi, and O, atoms are represented by the yellow, light purple, brown, black purple and red balls, respectively.

3. Results and discussion

3.1. X-ray diffraction (XRD)

Figure 4 displays the X-ray diffraction of the synthesized materials pure "BiOBr, BiOBr@xKaol (x= 0.2, 0.4, 0.6, 0.8 and 1) and raw kaolinite". The XRD patterns of the raw kaolinite are represented in black, it can be observed that the diffraction peaks located at 2θ = 12.35°, 20.35°, 24.85°, 26.6°, 37.7°, and 62.25° were assigned to the planes (001), (110), (002), (003), and (031) according to the card (JCPDS No. 96-900-9235). XRD patterns of the pure BiOBr showed the principal diffraction peaks situated at 2θ=10.9°, 21.92°, 25.19°, 31.71°, 32.24°, 39.32°, 44.66°, 46.17°, 46.90°, 47.64°, 50.66°, 53.34°, 56.10°, 57.18°, 61.85°, 66.28°, and 67.48°, which were assigned to (001), (002), (101), (102), (110), (112), (004), (200), (113), (201), (104), (211), (114), (212), (105), (204), and (220) lattice planes, respectively. This is indexed to the Tetragonal structure according to the (JCPDS card no. 01-078-0348). However, it can be seen from the plots of all the mass ratio of photocatalytic nanocomposites that as the mass of kaolinite increases, the peak intensity of the plans (001), (002), (101), (102), of the BiOBr phase, and (001), (002), of the kaolinite also increases. This increment can be explained by the increased crystalline due to the increasing amount of kaolinite [40,44]. In addition, the intensity of BiOBr peaks was always higher than those of kaolinite peaks, and some peaks of kaolinite were missing in all nanocomposites, indicating that the kaolinite surface was recovered by the BiOBr nanosheets, owing to the adsorption capacity of the layered aluminosilicate of kaolinite [45]. The results indicate that the nanocomposites were successfully synthesized.

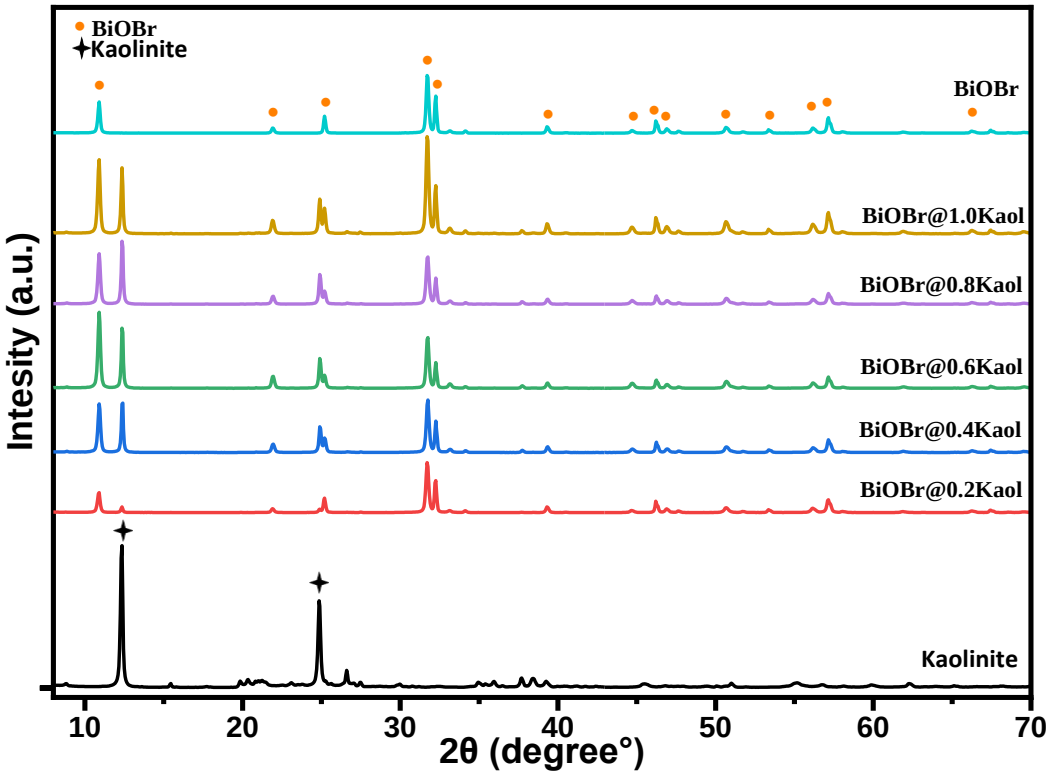

Figure 4: XRD of raw kaolinite and as-prepared photocatalysts.

3.2. Fourier transform infrared

Fourier transform infrared spectroscopy (FTIR) of raw kaolinite, pure BiOBr and as-synthesized BiOBr@Kaol are investigated in the range of 400–4000 cm^{-1} (**Figure 5**). The spectra of raw kaolinite (**Figure 5a**), showed the characteristics band at 3618.45 cm^{-1} and 3697.54 cm^{-1} which is attributed to the stretching vibration mode of Aluminum hydroxide (Al–OH) and silicon hydroxide (Si–OH) group, respectively [24]. The characteristics peaks at 1116 cm^{-1} and 1007 cm^{-1} are allocated to the stretching vibration mode of Si–O group. The bands at 536 cm^{-1} and 785 cm^{-1} are assigned to Al-O-Si deformation [46]. Furthermore, the characteristics bands located at 468.70 cm^{-1} and 1029 cm^{-1} are associated by the deformation modes of Si-O-Si group [47]. The FT-IR spectra of pure BiOBr presented the characteristic peaks located at 421.37 cm^{-1} is attributed to vibration of Bi–Br. The detection of Bi-O functional group is confirmed by the characteristic band at 518 cm^{-1} [3]. The FT-IR spectrum of BiOBr@Kaol nanocomposites contains the functional groups of raw kaolinite and BiOBr confirmed the successful elaboration.

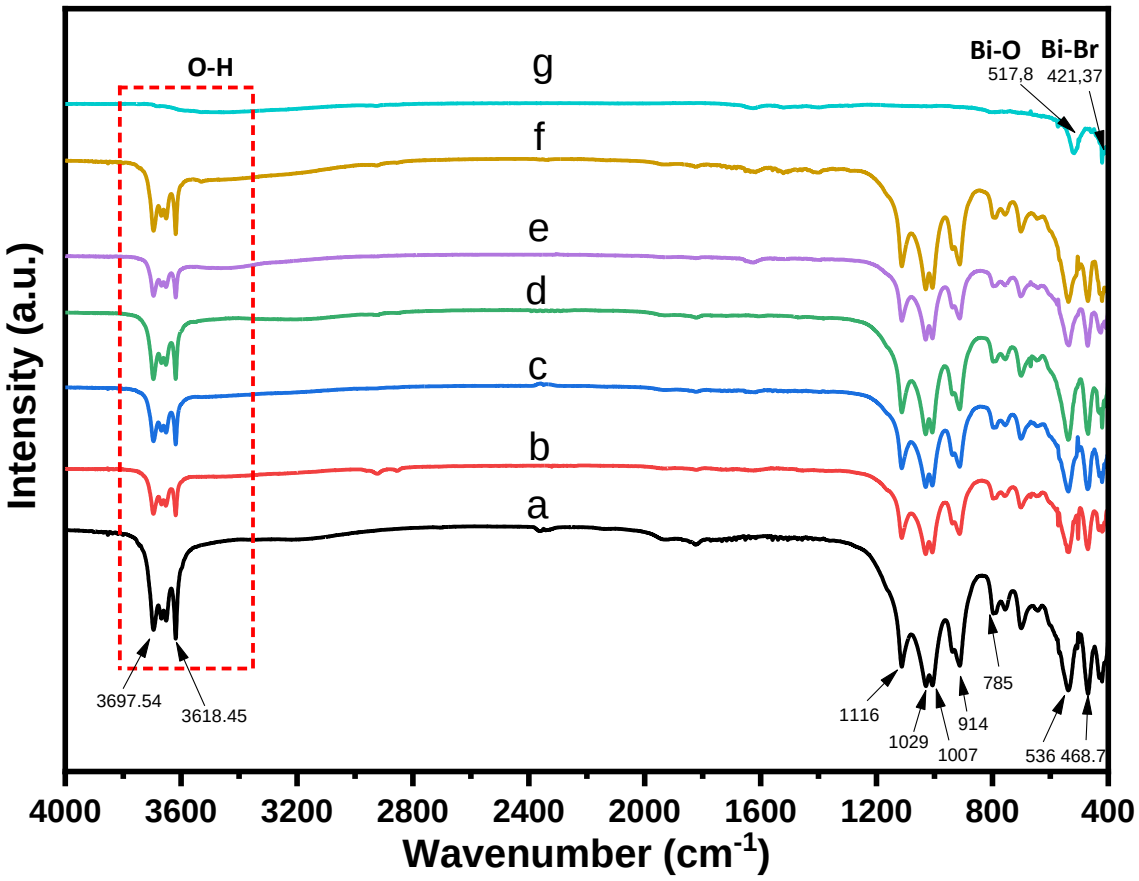

Figure 5: FT-IR spectra of raw kaolinite (a), BiOBr@0.2Kaol (b), BiOBr@0.4Kaol (c), BiOBr@0.6Kaol (d), BiOBr@0.8Kaol (e), BiOBr@1.0Kaol (f), and pure BiOBr (g).

3.3. Scanning electron microscopy & high resolution TEM

Figure 6 shows the surface image and elementary compositions of raw kaolinite and as-synthesized photocatalyst, as investigated by scanning electron microscopy and energy-dispersive X-ray spectroscopy (EDX). The SEM image and EDX spectrum of kaolinite clay mineral exhibits a stacking of many micro-sized layered structures of alumina octahedron and siloxane tetrahedron, the elementary composition of raw kaolinite is Al, Si, and O, which are well dispersed (as can be seen in **Figure** 5(a, b, c). Moreover, the SEM image of pure BiOBr displayed in **Figure 6d** and **6e**, showed the assembled of many with a morphology similar to that of a lotus flower, with diameter size about 3–6.2 µm. In addition, the EDX spectrum and mapping micrographic of pure BiOBr (**Figure 6f))**, indicated that the proportion of element Bi, O, and Br are equal and evenly dispersed. The SEM image of nanocomposite BiOBr@0.4Kaol, (**Figure 6g** and **6h)** showed that the BiOBr catalysis was supported on kaolinite surface. Additionally, EDX analysis and mapping image in **Figure 6-i,** revealed that the nanocomposite surface is homogenous due to the best distribution of all elements of pure BiOBr and raw kaolinite.

The micrograph in **Figure 6j** shows a 2D nanolayer of raw kaolinite in a pseudohexagonal form with a smooth and homogeneous surface. The diameter of these layers' ranges is between 400-900 nm. The TEM image in **Figure 6k** shows BiOBr holey nanosheets with a diameter size between 100 nm to 500 nm stacked together. Moreover, the TEM image in **Figure 6 l** clearly demonstrates that BiOBr nanosheets have been successfully dispersed on the surface of kaolinite.

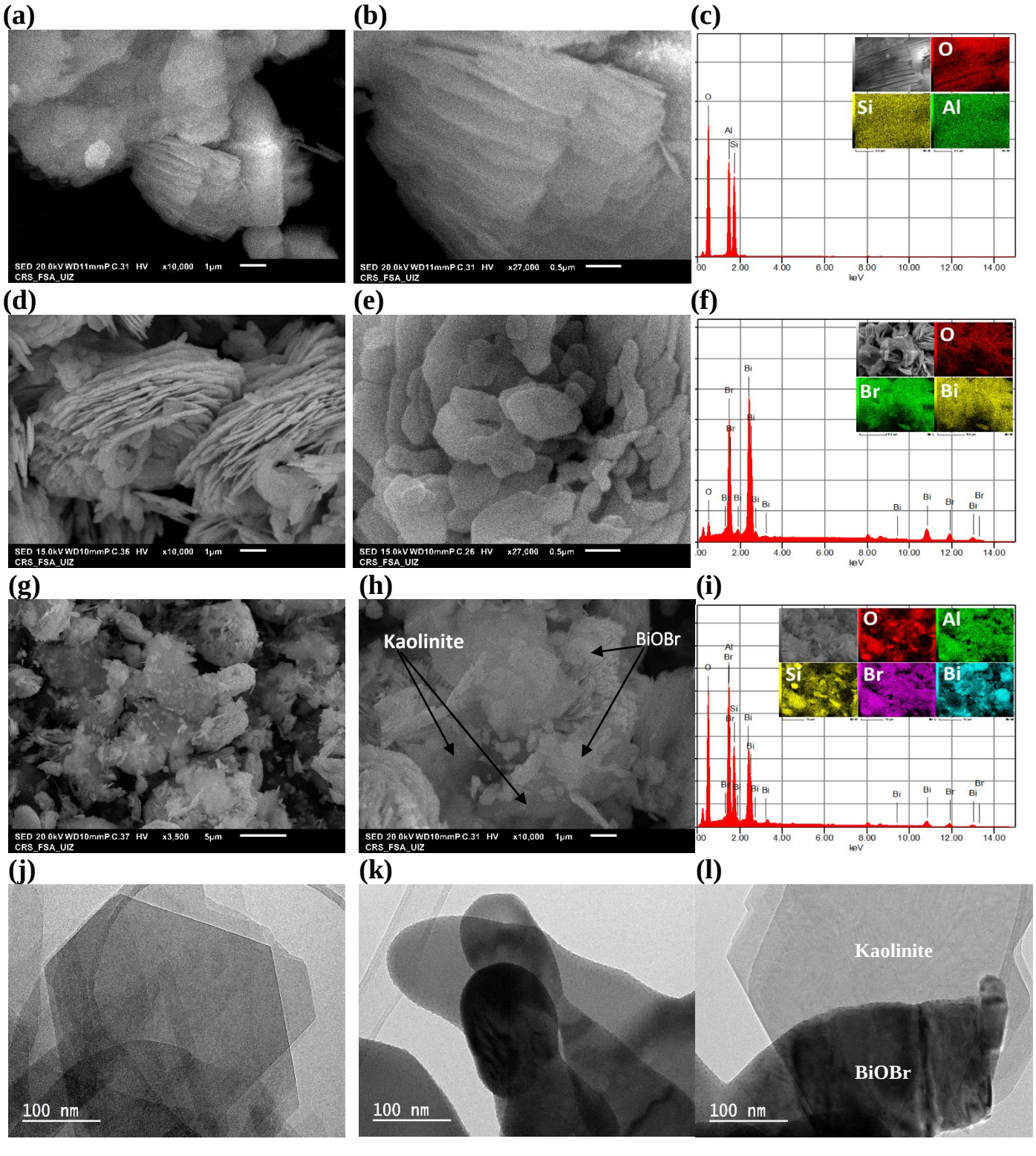

Figure 6: SEM image and EDX spectrum of raw kaolinite (a, b, c), pure BiOBr (d, e, f) Kaol@BiOBr (g, h, i). HRTEM of kaolinite (j), BiOBr (k) and BiOBr@Kaol (l).

3.4. Chemical state and surface structure analysis

The chemical compositions and chemical states of raw kaolinite, pure BiOBr and BiOBr@Kaol were analyzed using X-ray photoelectron spectroscopy (XPS) in the range of 0–1000 eV. **Figure 7** shows XPS spectra of BiOBr@Kaol, indicating the presence of Al, Si, O, Bi, Br and C elements. The high-resolution XPS spectra of Bi 4f exhibit two powerful peaks located at 157.1 eV and 162.4 eV corresponding to Bi^{3+} $4f_{7/2}$ and Bi^{3+} $4f_{5/2}$ orbitals of BiOBr in the BiOBr@Kaol composite, respectively (**Figure 7b**) [48]. The high-resolution XPS spectrum of Br 3d (**Figure 7c**), shows two peaks at binding energies of 65.5 eV and 66.5 eV, assigned to Br^{-1} $3d_{5/2}$ and Br^{-1} $3d_{3/2}$, respectively [49]. In **Figure 7d**, the high-resolution XPS spectrum of O 1s, exhibits two peaks at 528.6 eV and 530.5 eV, corresponding to the B-O and Bi-OH bands, respectively [24,50]. The high-resolution XPS spectrum of Al 2p (**Figure 7e**), shows two peaks at 735 eV and 74.3 eV ascribed the Al $2p_{1/2}$ an Al $2p_{3/2}$ orbitals sates. **Figure 7f,** presents the high-resolution XPS spectrum of Si 2p, where the observed peaks at binding energies 100.8 eV are depicted the Si-O-Si band [51].

Comparing the XPS spectra of pure BiOBr and BiOBr@Kaol (**Figure 7b** and **7d**), it is evident that the peaks corresponding to electronic states Bi^{3+} $4f_{7/2}$, Bi^{3+} $4f_{5/2}$ and O 1s (B-O band) exhibit a positive shift from 156.4 eV, 161.6 eV, and 527.1 eV, in pure BiOBr to 157.1 eV, 162.4 eV and 528.6 eV in BiOBr@Kaol, respectively. This shift can be attributed to the strong interfacial interaction between BiOBr and kaolinite [52,53]. The interaction between the two materials leads to hybridization of electronic states and charge transfer phenomena at the interface, resulting in changes in electron density and binding energies of the elements involved. Moreover, the shift of the, O 1s peak from 528.3 eV to 530.5 eV and the increased intensity of the Bi-OH band in confirm the a strong interaction between pure BiOBr and hydroxide groups in the kaolinite surface, indicating the successful synthesis of the BiOBr@Kaolinite composite.

As shown in **figure 7b**, two low intensity peaks located at the binding energies of 154 eV and 159.4 eV are corresponded to the Bi $4f_{7/2}$ and Bi $4f_{5/2}$ states of the bismuth element. However, in the case of BiOBr@Kaolinite, it is noted that the Bi $4f_{7/2}$ and Bi $4f_{5/2}$ feature peaks are not clearly observed. This could be attributed to several factors, including the modification of the kaolinite surface, interaction between the bismuth species and kaolinite, or changes in the

oxidation state of bismuth in the composite material. Further investigation and analysis are required to fully understand and explain the absence or alterations of these characteristic peaks in BiOBr@Kaolinite compared to pure BiOBr.

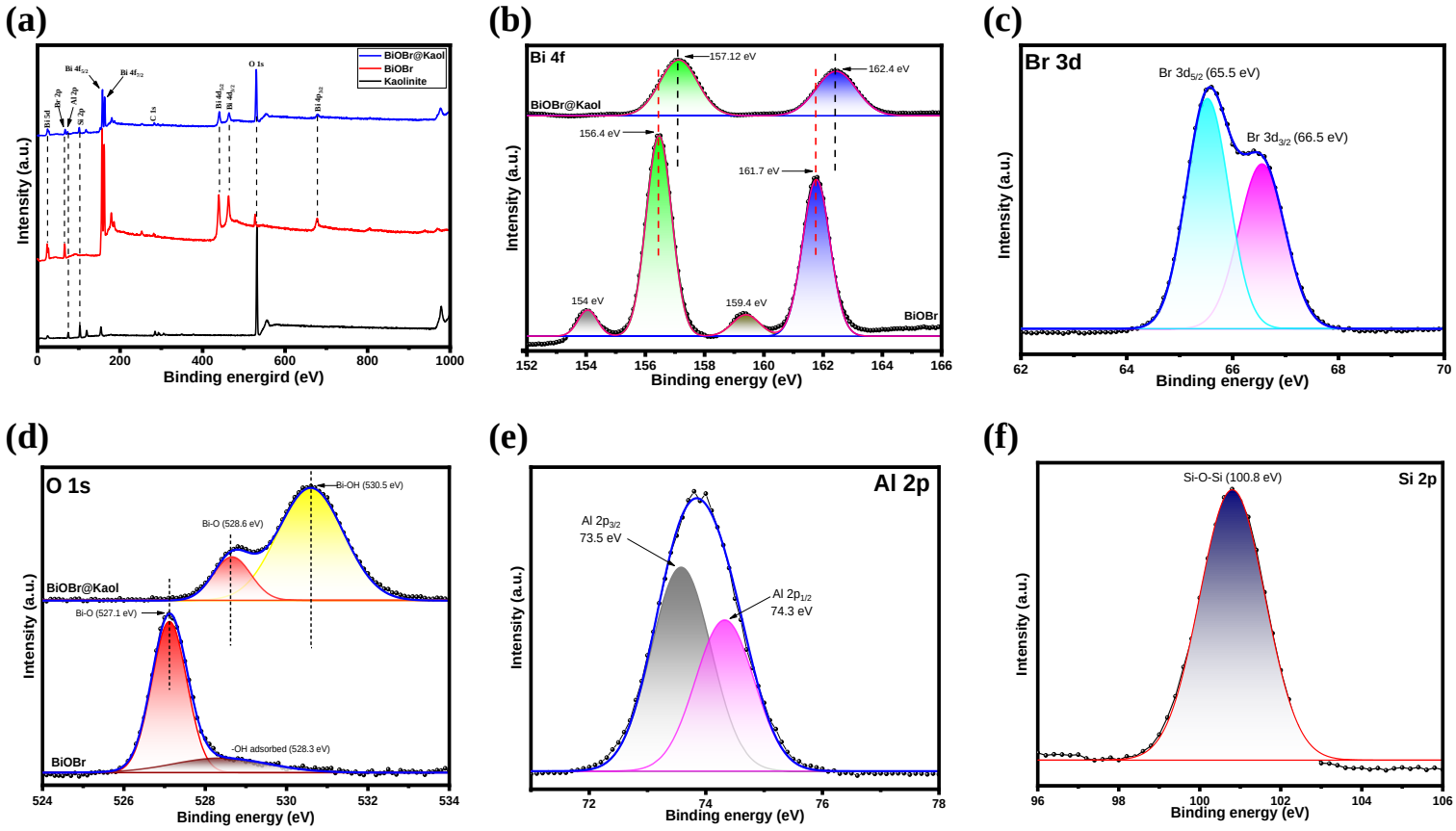

Figure 7: the XPS survery spectrum of raw kaolinite, BiOBr and BiOBr@Kaol (a), the high-resolution XPS of Bi 4f (b), Br 3d (c), O 1s (d), Al 2p (e), and Si 2p (f).

3.5. Optical properties and band gap energy

The band structure and band gap energy of semi-conductor are important indicators to evaluate the photocatalysis mechanism. **Figure 8** displays the UV–vis diffuse reflectance spectra (DRS) of as-synthesized photocatalyst. It can be seen from the **Figure 8a,** that the raw kaolinite, pure BiOBr, BiOBr@0.2Kaol, BiOBr@0.4Kaol, BiOBr@0.6Kaol, BiOBr@0.8Kaol and BiOBr@1.0Kaol exhibited an absorption edge at about 420, 475, 460, 450, 453, 455, 470 nm, respectively. This indicates that, all samples have a great absorption in the visible and UV regions. In addition, BiOBr@0.4Kaol has a best absorption boundary when compared with other samples. The data provided by UV-vis DRS were used to determinate the band gap energy of samples, using the following **equation 3**.

$$\alpha h\nu = \beta(h\nu - E_g)^{n/2} \qquad (3)$$

Where α, hv, β and Eg are the absorption coefficient, the photon energy, the band tailing parameter and the band gap energy, respectively. For the value of n, it depends on the property of the semiconductor (n=1 or 4 for direct band gap or indirect band gap separately). For a semiconductor with indirect band gap, BiOBr, the value of n is 4. The results were plotted in **Figure 8b**, the band gap energy (Eg) value of raw kaolinite, pure BiOBr, BiOBr@0.2Kaol, BiOBr@0.4Kaol, BiOBr@0.6aol, BiOBr@0.8Kaol, BiOBr@1.0Kaol, were 3.51, 2.79, 2.82, 2.69, 2.85, 2.83, and 2.75 eV. As shows from the results in **Figure 8b,** that the Eg value of BiOBr@0.4Kaol is the weakest, this decrease of the band gap energy is due to the increasing absorption rang of BiOBr@0.4Kaol.

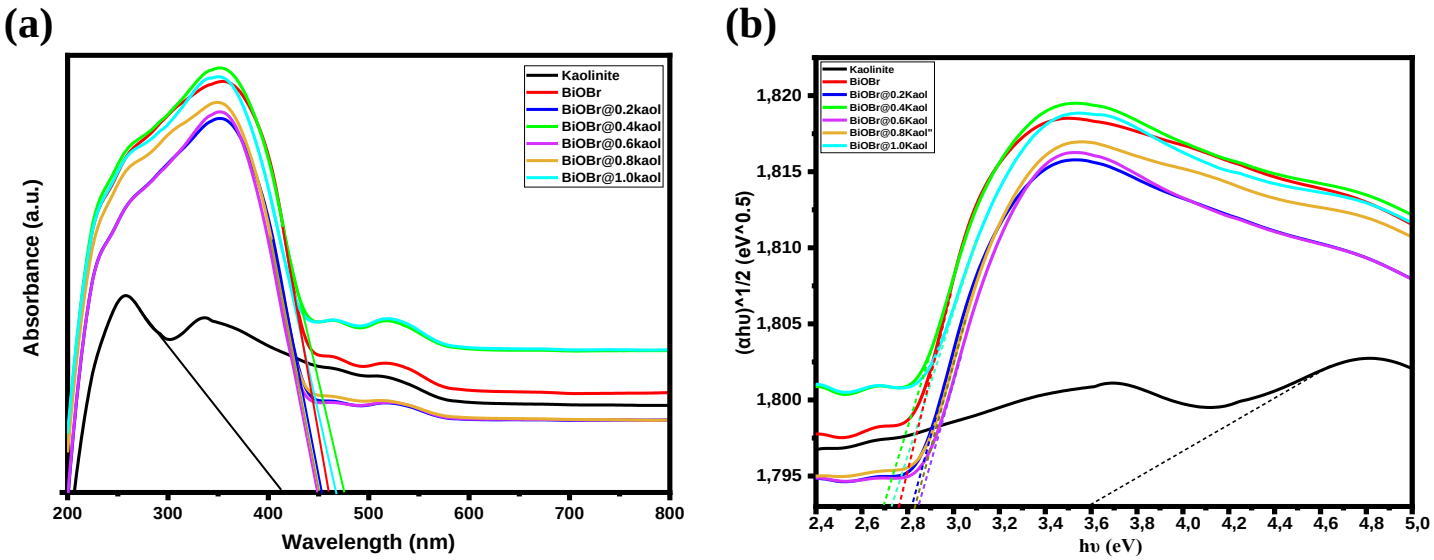

Figure 8: UV–vis diffuse reflectance spectra of raw kaolinite, pure BiOBr, BiOBr@0.2Kaol, BiOBr@0.4Kaol, BiOBr@0.6Kaol, BiOBr@0.8Kaol, BiOBr@1.0Kaol and (b) plot of $(\alpha hv)^2$ versus hv of as prepared sample.

3.6. Photocatalytic degradation study

The compared photocatalytic performance of as-prepared photocatalysts: pure BiOBr, BiOBr@1.0Kaol, BiOBr@0.8Kaol, BiOBr@0.6Kaol, BiOBr@0.4Kaol, and BiOBr@0.2Kaol, were investigated by employing 100 mL of RhB dye (10 ppm) with 100 mg of photocatalysts under sunlight irradiation. **Figure 9,** Shows the photolysis test, the adsorption-desorption equilibrium test, and photocatalytic degradation study. The degradation of RhB dye in aqueous solution was tested under sunlight irradiation. Before each photodegradation test, an adsorption-desorption equilibrium is applied for 60 min in dark condition (**Figure 9a**). The adsorption study of RhB dye into as-prepared BiOBr@0.4Kaol composite material demonstrated that the maximum removal efficiency did not exceed 29% after 60 min. After that, the rest solutions were exposed for further 30 min under sunlight irradiation using the as-prepared nanocomposites, the degradation efficiency for pure BiOBr,

BiOBr@1.0Kaol, BiOBr@0.8Kaol, BiOBr@0.6Kaol, BiOBr@0.4Kaol, BiOBr@0.2Kaol, and raw kaolinite, are 65.45%, 67.39%, 71.48%, 82.98%, 99.81%, 90.76%, and 6.28%, respectively (**Figure 9b**). It can be seen that the BiOBr@0.4Kaol nanocomposite has the best degradation efficiency (99.81%), this can be explained by the high separation performance of electron−hole pairs due to assembled of pure BiOBr and kaolinite clay. This suggested that electron–hole recombination is strongly decreased, which leads to strong photocatalytic performance. The experimental data also demonstrated that all BiOBr@Kaol nanocomposites have excellent degradation performance compared with pure BiOBr **Figure 9a**. It emphasizes that the interface between kaolinite and BiOBr plays a crucial role in facilitating efficient charge transfer and separation of photogenerated electron-hole pairs. This, in turn, reduces the recombination rate of the electron-hole pairs, leading to an enhancement in the photocatalytic activity of BiOBr. The findings highlight the significance of kaolinite modification as a key factor in improving the overall performance of BiOBr as a photocatalyst.

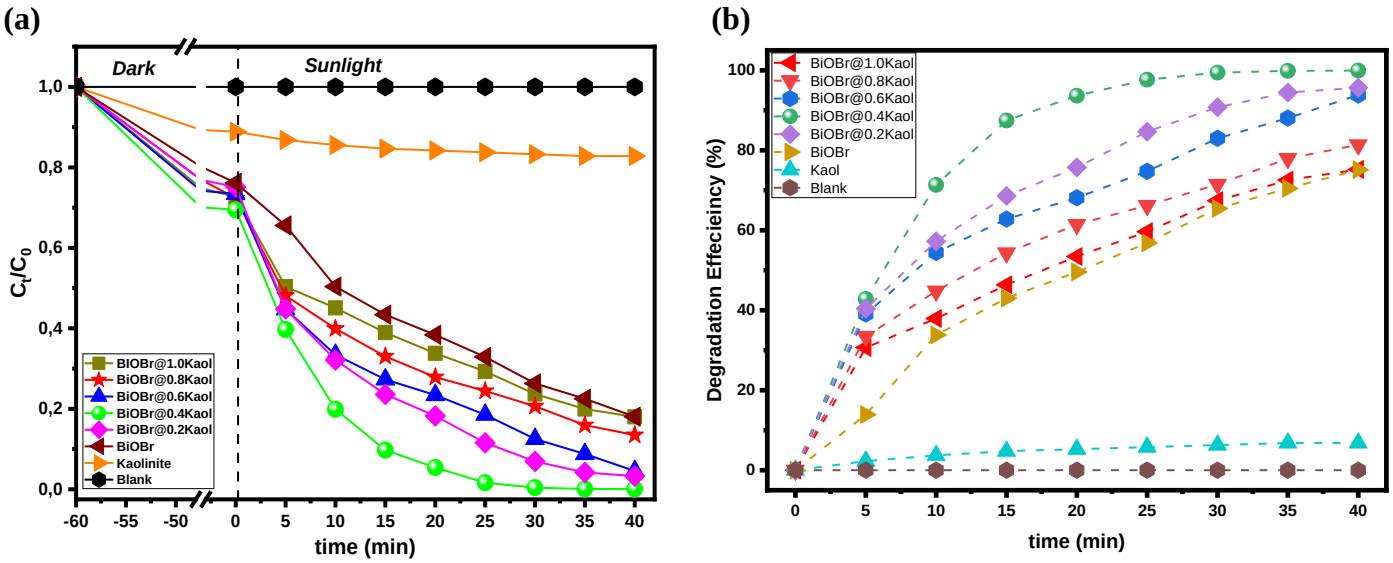

Figure 9: (a) adsorption and photocatalytic degradation of RhB dye under sunlight, (b) Degradation efficiency of RhB dye

The kinetic study is shown in **Figure 10.** The linear plots using the pseudo-first-order kinetic equation $\left(Ln\left(\frac{C_0}{C_t}\right) = K.t\right)$ of the as-synthesized samples are presented in **Figure 10a**. The kinetic rate constant is calculated from the slope of the previous equation. The rate constant K(min^{-1}) values of the as-prepared photocatalysts are presented in **Figure 10b**. It can be seen that the K values of all nanocomposites are superior of the rate constant of pure BiOBr, and the nanocomposite with 0.4 ratio presented the high rate constant (K= 0.1473 min^{-1}) which is

4.17 times more than of pure BiOBr (K=0.0353 min^{-1}). These results confirmed that the surface and structure of the kaolinite clay can be played an effective role to improve the speediness of degradation of RhB dye.

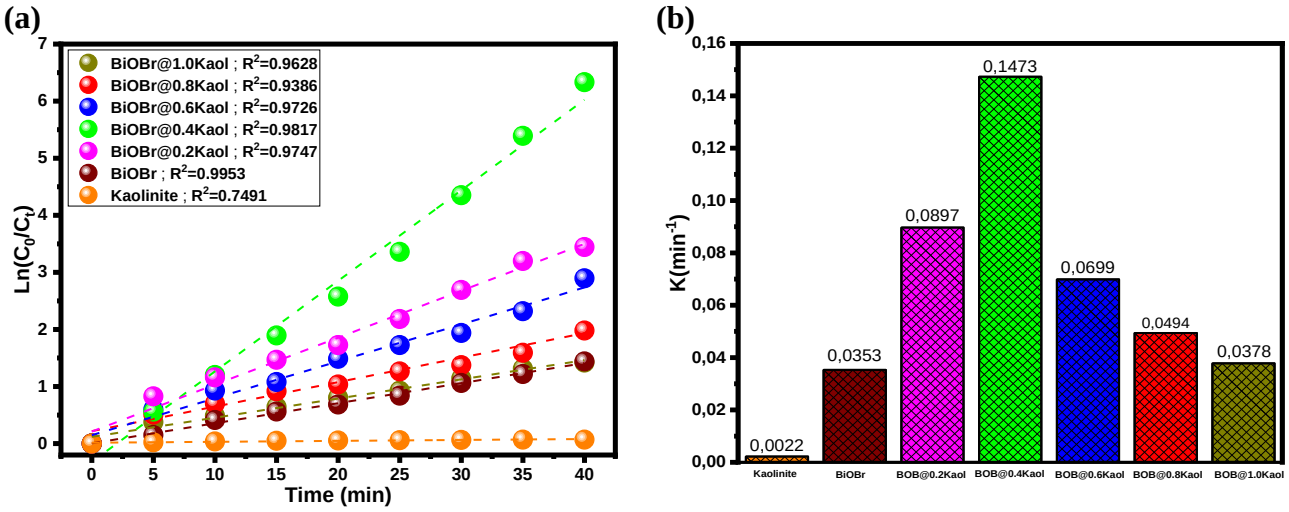

Figure 10: (a) Photocatalytic kinetic using first-order kinetic (b) The rate constant kinetic values

3.7. Calculation methods based on DFT-D and Monte Carlo

3.7.1. Quantum calculations

Based on the density functional theory (DFT-D), the BiOBr, Kaolinite and RhB species were optimized to obtain the structural relaxation based on the Perdew–Burke–Ernzerhof (PBE) functional in the Grimme (**Figure 11**). Total energy of Kaolinite, BiOBr and RhB was obtained -27740.463, -374.690 and -1880.764, Ha, respectively. The geometric parameters of Kaolinite, BiOBr and RhB are summarized in **Table 1**.

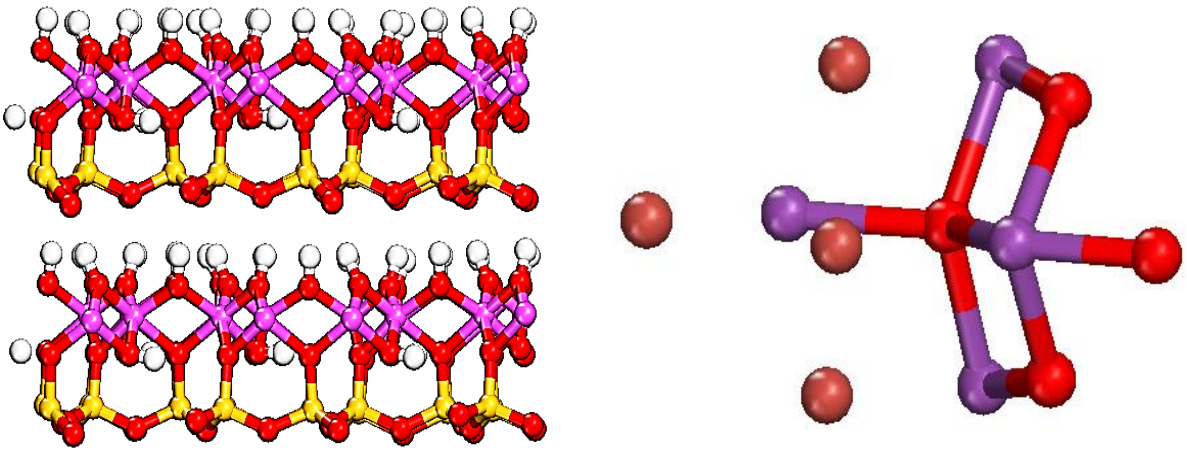

a **b**

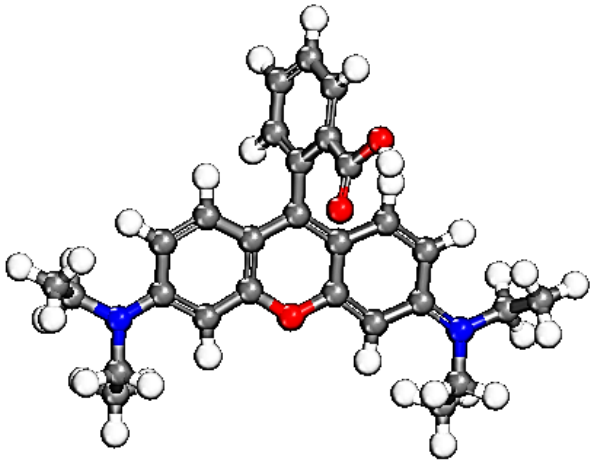

C

Figure 11: Optimized geometric structures of (a) dilayered Kaol, (b) BiOBr and (c) RhB dye.

Table 1. The geometric parameters of all compounds obtained by DMol^3 based on DFT-D.

	Kaolinite	**BiOBr**	**RhB**
Sum of atomic energies	-27686.708	-372.585	-1868.168
Kinetic	-126.215	-0.729	-18.431
Electrostatic	39.296	-2.237	-2.017
Exchange-correlation	20.682	0.348	4.536
Spin polarization	12.481	0.516	3.394
DFT-D correction	-	-0.002	-0.079
Total Energy	-27740.463	-374.690	-1880.764

3.7.2. Modelling by Monte Carlo adsorption locator simulation

After the optimization of compounds by quantum calculations, the lowest energy absorption of 5 BiOBr (001) species on Kaol (001) was investigated to make the BiOBr@Kaol heterojunction interface by adsorption locator module and force field; universal in Materials Studio 2017 software [54]. The electrostatic and van der Waals was calculated using the Group summation method.

The BiOBr (001) surfaces with Bi-, O- and Br-terminated can be adsorbed on Kaol surface. The adsorption energy (E_{ad}) of 5 molecules of BiOBr on Kaol was evaluated about -982.282 kcal/mol. In addition, BiOBr can be adsorbed approximately more on HO-Al surface (0 0 1) as compared with SiO-terminated surfaces (0 0 $\bar{1}$). The equilibrium configurations can be displayed in **Figure 12**. In other words, in the view of the configurations on kaolinite (0 0 1)

surface was located easier to coat on HO-Al surfaces than (0 0 $\bar{1}$) surface. The results showed that, Bi atoms of BiOBr were contributed to interact on HO-Al and SiO-terminated surfaces of kaolinite.

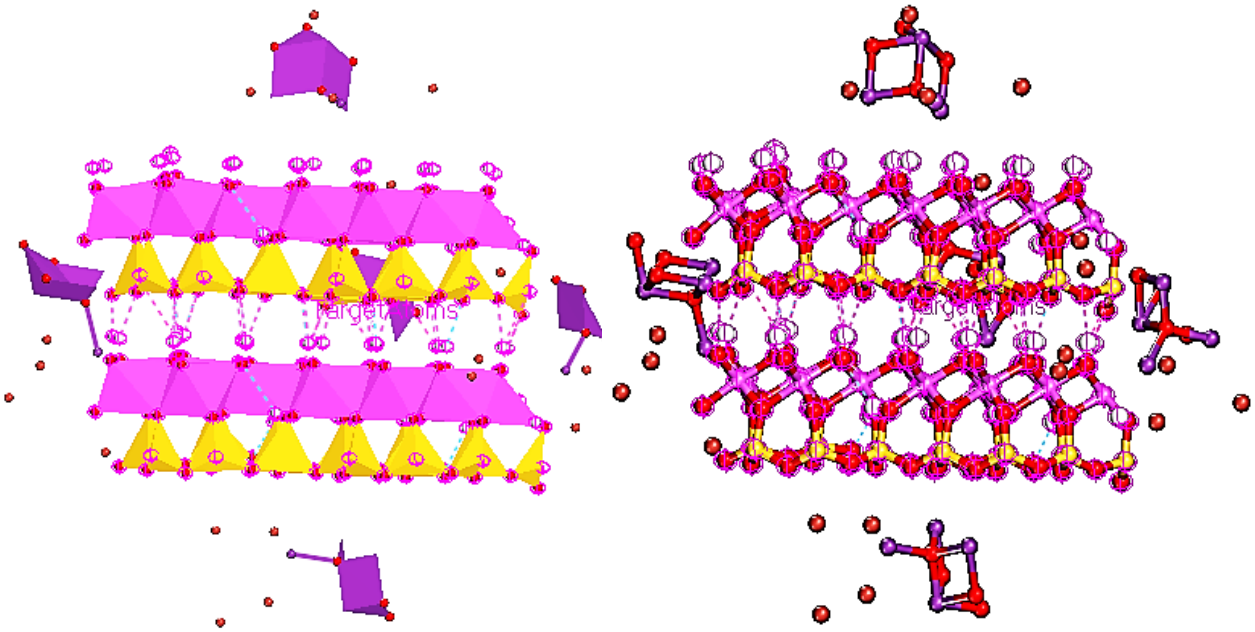

Figure 12: The lowest energy absorption of 5 BiOBr (001) species on Kaol (001) by adsorption locator module and forcefield; universal in Materials Studio 2017 software.

This work gives deep theoretical insights into the migration of RhB on the BiOBr(001)@Kaol(001) surface and provides new perspective for understanding the structure-performance relationship rule. Based on the preferential adsorption models of adsorbates (RhB) on BiOBr@Kaol heterojunction surface by Monte Carlo calculation, the total adsorption energies of 5 molecules and 3 molecules of the RhB for BiOBr@Kaol were obtained about -310.813 and -233.816 kcal/mol, respectively (**Figure 13**), demonstrating the exothermic and stability of the adsorption system owing to its high negative interaction energy [55,56]. On the basis of the above analyses, the negative values mean that the adsorbates can be adsorbed on the (0 0 1) surface. It also could be concluded that van der Waals attractions were responsible between the RhB molecules and BiOBr@Kaol surface. The negative adsorption energy Eads value of 5 molecules of the RhB on BiOBr@Kaol surface was larger than the 3 molecules of the RhB on BiOBr@Kaol surface, suggesting more adsorption of pollutants. In addition, by RhB adsorption on BiOBr@Kaol surface, bismuth oxybromide (BiOBr) as a typical layered visible light photocatalyst can be affected on the degradation of RhB.

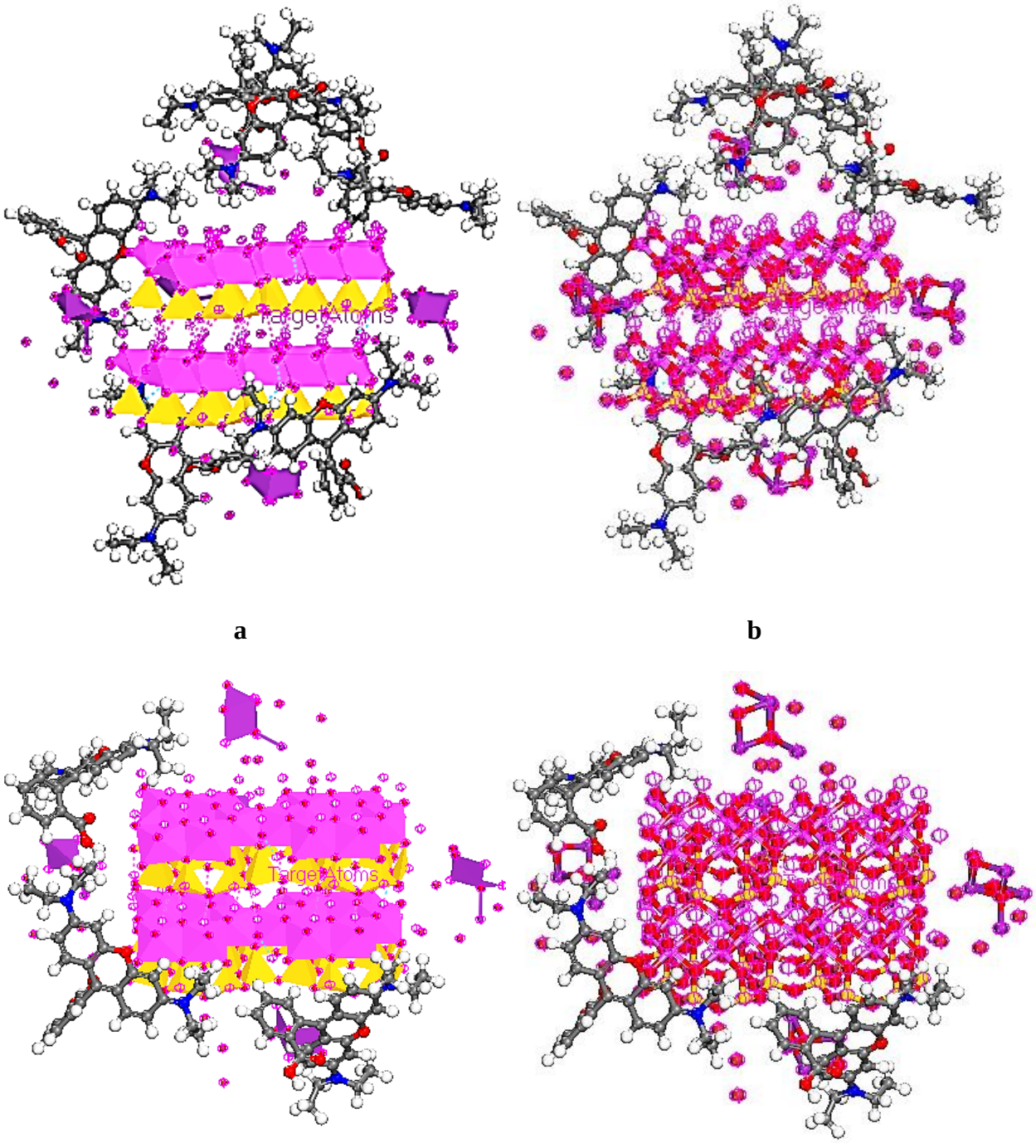

a **b**

c **d**

Figure 13. (a and b); The lowest adsorption energy of 5 RhB on Kaol (001) and (c and d); the lowest adsorption energy of 3 RhB on Kaol (001) by adsorption locator module and forcefield; universal in Materials Studio 2017 software.

DFT-D and MD were used to investigate the optimization of structures, BiOBr absorption on the kaolinite (0 0 1) surface and RhB adsorption on BiOBr@Kaol. The results indicated that the BiOBr adsorption was parallel on HO-Al surface of kaolinite (0 0 1) surface and (0 0 $\bar{1}$) surface. Meanwhile, the BiOBr adsorption on (0 0 $\bar{1}$) surface was relatively strong. In

addition, the adsorption of RhB species on the BiOBr@Kaol surface should be more stable due to the high negative interaction energy.

3.8. Possible Photocatalytic mechanism

The photocatalytic mechanism for the RhB degradation by BiOBr@Kaol nanocomposite under sunlight irradiation was investigated. The photocatalytic reaction was trapping using the actives species named scavengers; these scavengers play a crucial role to determine the radical species responsible for RhB oxidation in the photocatalytic reaction. Acid ascorbic (**ASC**), isopropanol alcohol (**IPR**), and ethylene diamine tetraacetic acid (**EDTA**), are the most commonly scavengers using to trapping radicals (**•O_2^-**), (**HO•**), and (**h^+**), respectively. In the typical process, 4 mmol of each scavenger was added in 50 mL RhB dye solution (10 ppm), with 50 mg of BiOBr@0.4Kaol and agitated under sunlight irradiation for 20 min. The solution was then collected and separated by centrifuge; the remaining dye concentration was determined using UV spectrophotometer. The experimental results of the scavenger's tests are presented in **Figure 14.** Whereas, the degradation efficiency of RhB dye is 95.3 %, 80.50 %, and 26% for as scavengers (**EDTA**), (**ASC**), and (**IPR**), respectively, demonstrating that the superoxide radicals (**•O_2^-**) is the active species responsible of the degradation of RhB dye and the h^+ hole has a relatively minor effect on the direct photodegradation of RhB molecules.

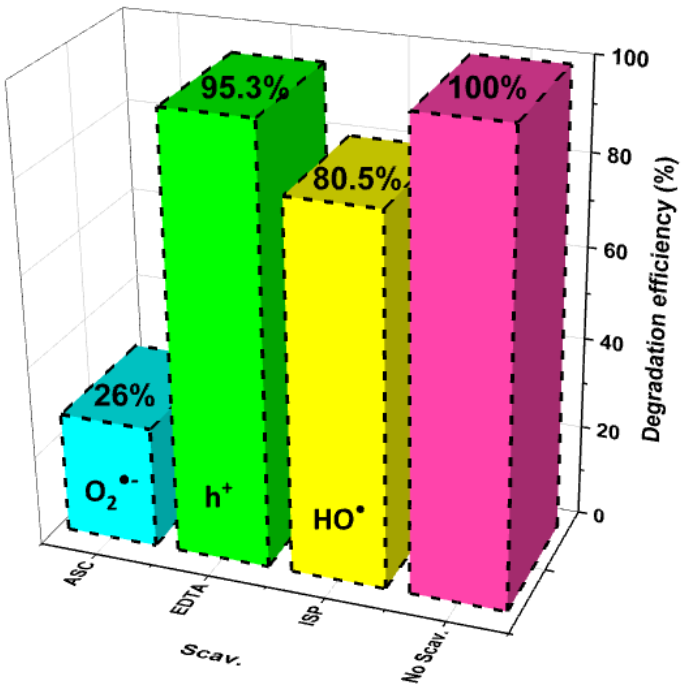

Figure 14. The actives species trapping experiments for degradation efficiency of RhB dye by BiOBr@Kaol

In addition, the BC and BV edge potentials of BiOBr@Kaol semiconductor are calculated using the following equations [36].

$$\chi(A_aB_bC_c) = [\chi A^a . \chi B^b . \chi C^c]^{\frac{1}{a+b+c}} \quad \textbf{(4)}$$

$$E_{BC} = \chi(A_aB_bC_c) - E_0 - \frac{E_g}{2} \quad \textbf{(5)}$$

$$E_{BV} = E_{BC} + E_g \quad \textbf{(6)}$$

Where χ(eV) is the absolute electronegativity of the semiconductor BiOBr, and a, b, and c are the number of atoms in a chemical formula $A_aB_bC_c$. E_{VB} (eV), E_{CB}, and Eg (eV) are the VB edge potential, CB edge potential, and the band gap energy of the semi-conductors respectively. E_0 (eV) is the energy of free electrons on the hydrogen scale ($E_0 \approx 4.5$ eV/NHE). **Table 2** summarized the calculated χ of BiOBr@Kaol, E_{VB}, E_{CB}, edge potential and Eg of BiOBr@Kaol.

Table 2: Calculation results of the E_{CB} and E_{VB} potentials of BiOBr semiconductor.

Semiconductors	**χ(eV)**	**Eg**	**E_{CB}**	**E_{CV}**
BiOBr	6.45	2.79	0.5	3.29

The photocatalytic mechanism of RhB dye degradation over the BiOBr@Kaol nanocomposite under sunlight irradiation is depicted in **Figure 15.** When the semiconductor is excited by solar radiation, an electron (e-) from the valence band edge (E_{CV}) transfers to the conduction band edge (E_{CB}), generating a hole (h+) in the valence band (VB) and forming an electron-hole pair (**Equation 7**). The (e^- and h^+) pairs oxidize water molecules to hydroxyl radicals (**$OH^•$**) using hole (h^+), (**Equation 8**) and reduce the oxygen to the superoxide radicals (**$•O_2^-$**) through electron (e^-), (**Equation 9**). These generated radicals are responsible for degrading the RhB molecules to H_2O and CO_2 as shown in (**Equation 10).** Additionally, the strong adsorptive properties and negatively charged surface of kaolinite clay play a crucial role to improve the photocatalytic performance. The electrostatic attraction between the photogenerated holes at the E_{VB} edge and the negatively charged kaolinite surface effectively prevents recombination of the electron-hole pairs. Therefore, the free holes in the E_{VB} are occupied by the negative charge of the kaolinite, further enhancing the separation of photogenerated electrons and holes. This process significantly improves the photodegradation efficiency of RhB dye over the BiOBr@Kaol photocatalyst. The potential mechanism of the RhB photodegradation reaction by BiOBr@Kaol is illustrated in **Figure 15**.

$$\text{BiOBr@Kaol} + h\upsilon = e_{CB}^{-} + h_{VB}^{+} \quad \textbf{(7)}$$

$$h_{VB}^{+} + H_2O = \bullet OH \quad \textbf{(8)}$$

$$e_{CB}^{-} + O_2 = \bullet O_2^{-} \quad \textbf{(9)}$$

$$\bullet O_2^{-} \text{ or } \bullet OH + RhB = CO_2 + H_2O \quad \textbf{(10)}$$

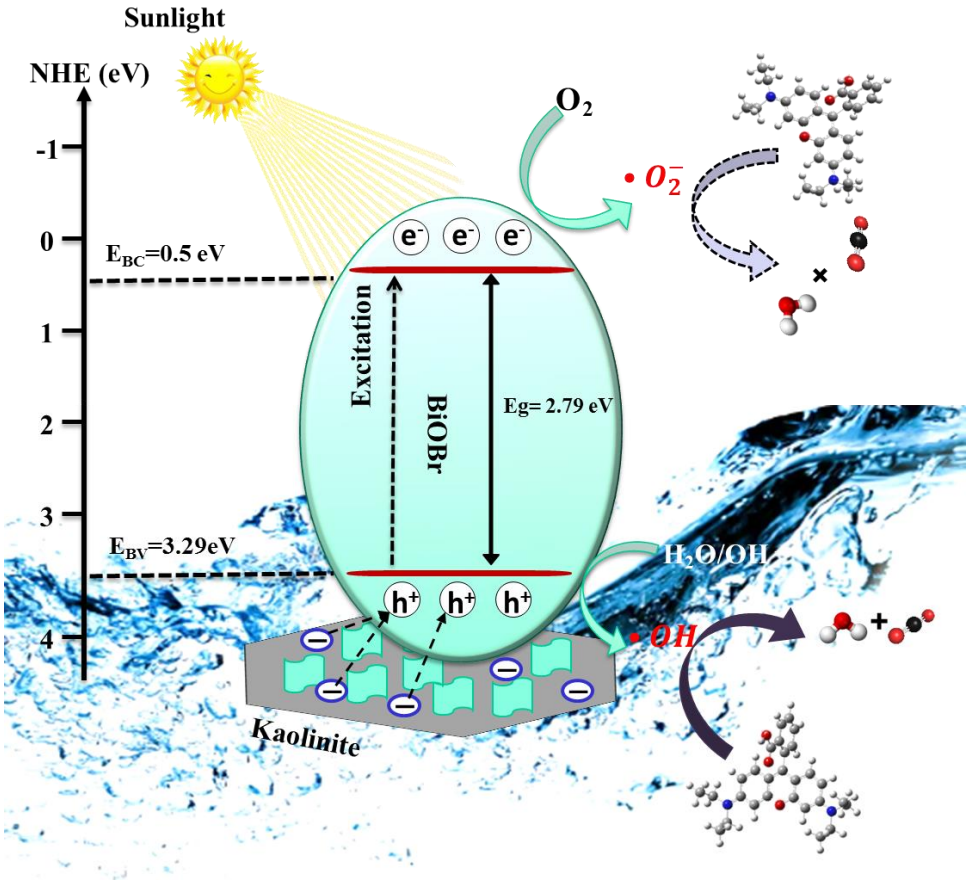

Figure 15: Proposal mechanisms of degradation of RhB dye by BiOBr@Kaol nanocomposite under sunlight.

3.9. Stability and reusability of the photocatalyst

The evaluation of the durability of photocatalyst is very important index for their practical applications in large-scale. In typical protocol, the BiOBr@Kaol and pure BiOBr were used in first application to degrade RhB dye, after the first demineralization, the powder BiOBr@Kaol and pure BiOBr were collected using centrifuge, washed several times by deionized water and acetone, dried in the oven at 75 °C for 12 hours and used for the next

application. The regeneration of BiOBr@Kaol was realized in five cycles. As can be seen in **Figure 16-a**, the degradation efficiency of RhB dye by BiOBr@Kaol is slightly decreased from 100% to 97.99% after five cycles compared with pure BiOBr, which has a degradation efficiency strongly decreased from 81.96% to 20.45%. In addition, the SEM image of the BiOBr@0.4Kaol nanocomposite after five cycles of reuse (**Figure 16, b**) clearly shows that the material remains stable and its morphology unchanged. Furthermore, the EDX spectrum and mapping micrograph of BiOBr@0.4Kaol after five cycles of reuse (**Figure 16, c**) indicate that the nanocomposite surface is homogeneous and that all elements of pure BiOBr and raw kaolinite are evenly dispersed. It also mentions the absence of impurity peaks, providing important insights into the nanocomposite structural integrity. This indicates that the agglomeration issue of the BiOBr semiconductor has been successfully solved. Thus, the results are very promising for large-scale application.

(a)

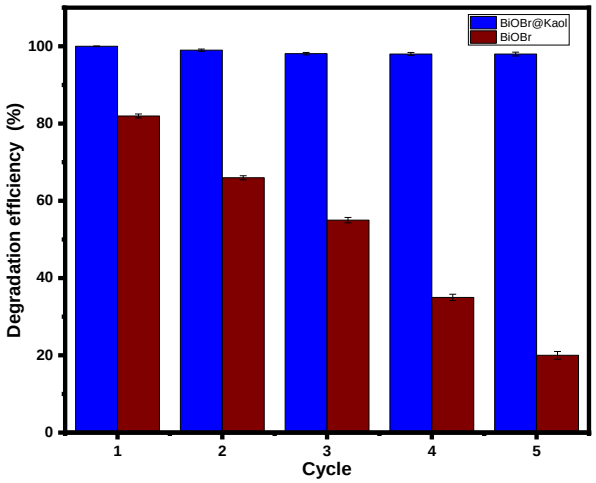

(b)

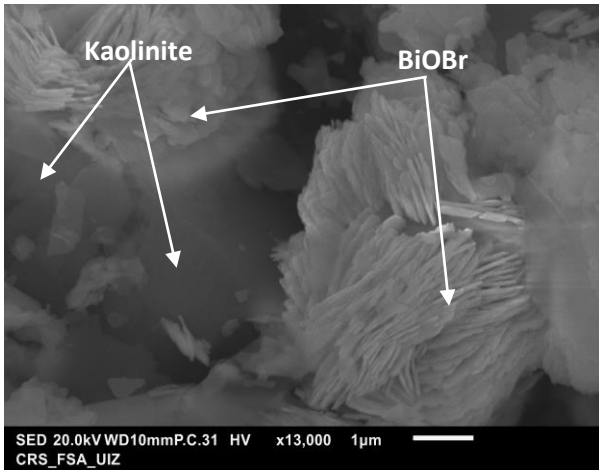

(c)

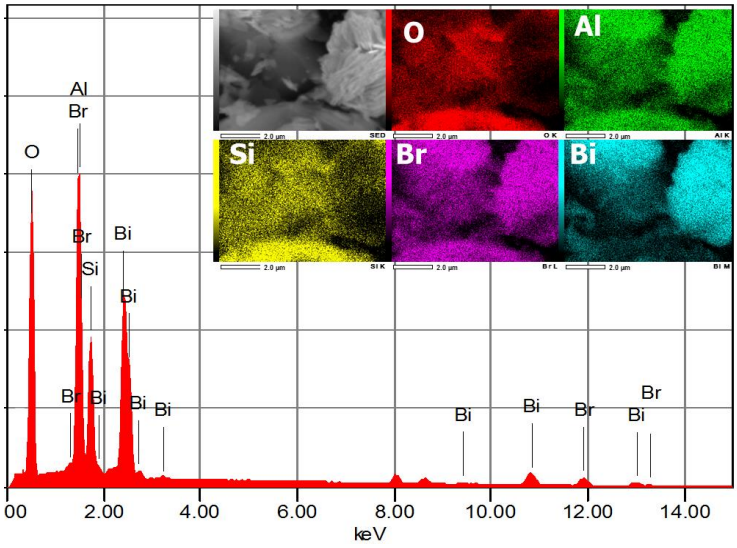

Figure 16: Cyclic rune experiment of BiOBr@0.4Kaol nanocomposite and pure BiOBr for RhB degradation (a), SEM and EDS mapping images of BiOBr@0.4Kaol nanocomposite after five reuse cycles (b and c).

3.10. Comparison study

To confirm the reliability of the synthesized nanocomposites, the degradation efficiency of RhB dye by BiOBr@Kaol was compared with other highly efficient photocatalysts reported in the literature (**Table 3**). When the pure BiOBr catalyst was modified with Kaolinite clay, the photodegradation performance of RhB dye was remarkably enhanced and reached 100% compared with Metal doped BiOBr or heterojunction with another semiconductor. These results can be applied by utilizing kaolinite clay for synthesis of other nanocomposites with different semiconductor photocatalysts in order to achieve higher photocatalytic performance.

Table. 3: Comparison between BiOBr@Kaol and other composites materials for RhB dye photodegradation.

Photocatalysts	Condition	Light source	Degradation Efficiency (%)	Time (min)	Reference
2.0% gC_3N_4/ BiOBr	60.0 mg, 60.0 mL * 10.0 mg L^{-1}	visible light	98%	150	[57]
Y-doped BiOBr	10 mg, 100 mL * 10 mg L^{-1}	Visible light	98%	60	[58]
Bi-BiOBr/$BiPO_4$	50 mg, 100 mL * 10 mg L^{-1}	Visible light	89.7%	90	[59]
Mt/ZnO	100 mg, 100 mL * 10 mg L^{-1}	UV-light	95%	70	[60]
Bentonite /Nb_2O_5	120 mg, 250 mL * 30 mg L^{-1}	UV light	98%	120	[61]
BiOBr/ZnWO4	100 mg, 100 mL * 1.0×10^{-5} mol L^{-1}	UV light	98.3%	25	[62]
BiOBr-Au-CdS	50 mg, 50 mL * 20 mg/L	Sunlight	100%	50	[63]
BiOBr@Kaol	100 mg, 100 mL * 10 mg/L	Sunlight	100%	30	This work
Pure BiOBr	100 mg, 100 mL * 10 mg/L	Sunlight	81.96%	40	This work

4. Conclusion

It summarizes the findings of the study and draws conclusions based on the results. It states that the BiOBr@Kaol nanocomposite with a mass ratio of 0.4 kaolinite exhibited the highest photocatalytic efficiency for RhB degradation, achieving 100% dye decomposition within 30 minutes under sunlight irradiation. It also mentions that the degradation rate of BiOBr@0.4Kaol was 4.17 times higher than that of pure BiOBr, indicating improved separation of photogenerated electron-hole pairs. Furthermore, to investigate the adsorption mechanisms of BiOBr on kaolinite particles and RhB molecules on BiOBr@Kaol, DFT-D and MD simulations were employed. The MD simulations and Monte Carlo calculations revealed that the BiOBr molecules aligned approximately parallel to the surfaces of kaolinite particles that contained -OH groups. Specifically, one of the (001) kaolinite surfaces, which carried OH groups, formed hydrogen bonds with the BiOBr-O atoms. Additionally, the results indicated that the interactions between RhB molecules and BiOBr@Kaol were of the Van der Waals type. Importantly, the adsorption energies of BiOBr on kaolinite particles and RhB molecules on BiOBr@Kaol were determined to be negative, indicating a stable and exothermic system. The facile synthesis of the photocatalyst holds promising potential for large-scale water remediation applications.

Acknowledgements:

This work results from a collaborative effort between involving scientific members of Faculté des Sciences d'Agadir, Faculté des Sciences Appliquées d'Ait Melloul, Université Ibn Zohr, Agadir Morocco, and Institut de Sciences des Matériaux de Mulhouse (IS2M-UMR 7361 CNRS), Université de Haute Alsace (UHA), Mulhouse-France. We thank VIDAL Loïc (IS2M-MulhouseFrance), VAULOT Cyril (IS2M-Mulhouse-France), GREE Simon (IS2M-Mulhouse-France) and FIOUX Philippe (IS2M-Mulhouse-France), for the Transmission electron microscopy (TEM), the Ultraviolet–Visible Diffuse Reflectance Spectroscopy (UV–Vis DRS), the Fourier-transform infrared spectroscopy (FT-IR), and the X-Ray photoelectron spectrometry analyzes, respectively.

References

[1] R. Haounati, H. Ouachtak, R. El, S. Akhouairi, F. Largo, Elaboration and properties of a new SDS/CTAB@Montmorillonite organoclay composite as a superb adsorbent for the removal of malachite green from aqueous solutions, Sep. Purif. Technol. 255 (2021) 117335. https://doi.org/10.1016/j.seppur.2020.117335.

[2] H. Ighnih, R. Haounati, H. Ouachtak, A. Regti, B. El Ibrahimi, N. Hafid, A. Jada, M. Labd Taha, A.A. Addi, Efficient removal of hazardous dye from aqueous solutions using magnetic kaolinite nanocomposite: Experimental and Monte Carlo simulation studies, Inorg. Chem. Commun. 153 (2023) 110886. https://doi.org/10.1016/j.inoche.2023.110886.

[3] K. Liu, Z. Tong, Y. Muhammad, G. Huang, H. Zhang, Z. Wang, Y. Zhu, R. Tang, Synthesis of sodium dodecyl sulfate modified BiOBr/magnetic bentonite photocatalyst with Three-dimensional parterre like structure for the enhanced photodegradation of tetracycline and ciprofloxacin, Chem. Eng. J. 388 (2020) 124374. https://doi.org/10.1016/j.cej.2020.124374.

[4] H. Ouachtak, R. El, A. El, R. Haounati, E. Amaterz, A. Ait, F. Akbal, M. Labd, Experimental and molecular dynamics simulation study on the adsorption of Rhodamine B dye on magnetic montmorillonite composite γ -Fe 2 O 3 @ Mt, J. Mol. Liq. 309 (2020) 113142. https://doi.org/10.1016/j.molliq.2020.113142.

[5] F. Alakhras, E. Alhajri, R. Haounati, H. Ouachtak, A. Ait, A. Saleh, A comparative study of photocatalytic degradation of Rhodamine B using natural-based zeolite composites, Surfaces Interfaces J. 20 (2020). https://doi.org/10.1016/j.surfin.2020.100611.

[6] M. Ahmad, M. Tauseef, W. Rehman, N.H. Alotaibi, A. Gul, R.S. Abdel, M. Al, M.F.H. Abd, M. Nawaz, R. Ullah, Enhanced photocatalytic degradation of RhB dye from aqueous solution by biogenic catalyst Ag@ZnO, J. Alloys Compd. 895 (2022) 162636. https://doi.org/10.1016/j.jallcom.2021.162636.

[7] H. Ouachtak, A. El Guerdaoui, R. Haounati, S. Akhouairi, R. El Haouti, N. Hafid, A. Ait Addi, B. Šljukić, D.M.F. Santos, M.L. Taha, Highly efficient and fast batch adsorption of orange G dye from polluted water using superb organo-montmorillonite: Experimental study and molecular dynamics investigation, J. Mol. Liq. 335 (2021)

116560. https://doi.org/10.1016/j.molliq.2021.116560.

[8] H. Ouachtak, S. Akhouairi, R. Haounati, A.A. Addi, A. Jada, M.L. Taha, J. Douch, 3,4-dihydroxybenzoic acid removal from water by goethite modified natural sand column fixed-bed: Experimental study and mathematical modeling, Desalin. Water Treat. 194 (2020) 439–449. https://doi.org/10.5004/dwt.2020.25562.

[9] H. Ouachtak, A. El Guerdaoui, R. El Haouti, R. Haounati, H. Ighnih, Y. Toubi, F. Alakhras, R. Rehman, N. Hafid, A.A. Addi, M.L. Taha, Combined molecular dynamics simulations and experimental studies of the removal of cationic dyes on the eco-friendly adsorbent of activated carbon decorated montmorillonite Mt@AC, RSC Adv. 13 (2023) 5027–5044. https://doi.org/10.1039/D2RA08059A.

[10] F. Largo, R. Haounati, H. Ouachtak, N. Hafid, A. Jada, A.A. Addi, Design of organically modified sepiolite and its use as adsorbent for hazardous Malachite Green dye removal from water, Water. Air. Soil Pollut. 234 (2023) 1–17. https://doi.org/10.1007/S11270-023-06185-Z/METRICS.

[11] A. Imgharn, H. ighnih, A. Hsini, Y. Naciri, M. Laabd, H. Kabli, M. Elamine, R. Lakhmiri, B. Souhail, A. Albourine, Synthesis and characterization of polyaniline-based biocomposites and their application for effective removal of Orange G dye using adsorption in dynamic regime, Chem. Phys. Lett. 778 (2021) 138811. https://doi.org/10.1016/j.cplett.2021.138811.

[12] C. Zhao, J. Zhou, Y. Yan, L. Yang, G. Xing, H. Li, P. Wu, M. Wang, H. Zheng, Application of coagulation/flocculation in oily wastewater treatment: A review, Sci. Total Environ. 765 (2021) 142795. https://doi.org/10.1016/j.scitotenv.2020.142795.

[13] A. Yusaf, M. Usman, A. Mansha, M. Saeed, M. Ahmad, M. Siddiq, Micellar-enhanced ultrafiltration (MEUF) for removal of rhodamine B (RhB) from aqueous system, J. Dispers. Sci. Technol. 43 (2022) 366–348. https://doi.org/10.1080/01932691.2020.1841002.

[14] D.B. Miklos, C. Remy, M. Jekel, K.G. Linden, J.E. Drewes, U. Hübner, Evaluation of advanced oxidation processes for water and wastewater treatment – A critical review, Water Res. 139 (2018) 118–131. https://doi.org/10.1016/j.watres.2018.03.042.

[15] D. Kanakaraju, B.D. Glass, M. Oelgemöller, Advanced oxidation process-mediated removal of pharmaceuticals from water: A review, J. Environ. Manage. 219 (2018)

189–207. https://doi.org/10.1016/j.jenvman.2018.04.103.

[16] D. Ma, H. Yi, C. Lai, X. Liu, X. Huo, Z. An, L. Li, Y. Fu, B. Li, M. Zhang, L. Qin, S. Liu, L. Yang, Critical review of advanced oxidation processes in organic wastewater treatment, Chemosphere. 275 (2021) 130104. https://doi.org/10.1016/j.chemosphere.2021.130104.

[17] R. Haounati, F. Alakhras, H. Ouachtak, T.A. Saleh, G. Al-Mazaideh, E. Alhajri, A. Jada, N. Hafid, A.A. Addi, Synthesized of Zeolite@Ag2O Nanocomposite as Superb Stability Photocatalysis Toward Hazardous Rhodamine B Dye from Water, Arab. J. Sci. Eng. (2022). https://doi.org/10.1007/s13369-022-06899-y.

[18] N. López, P. Marco, J. Giménez, S. Esplugas, Photocatalytic diphenhydramine degradation under different radiation sources: Kinetic studies and energetic comparison, Appl. Catal. B Environ. 220 (2018) 497–505. https://doi.org/10.1016/J.APCATB.2017.08.077.

[19] F. Méndez-Arriaga, S. Esplugas, J. Giménez, Photocatalytic degradation of non-steroidal anti-inflammatory drugs with TiO2 and simulated solar irradiation, Water Res. 42 (2008) 585–594. https://doi.org/10.1016/J.WATRES.2007.08.002.

[20] G. Zhao, J. Zou, J. Hu, X. Long, F. Jiao, A critical review on graphitic carbon nitride (g-C 3 N 4) -based composites for environmental remediation, Sep. Purif. Technol. 279 (2021) 119769. https://doi.org/10.1016/j.seppur.2021.119769.

[21] P. Tun, K. Wang, H. Naing, J. Wang, G. Zhang, Facile preparation of visible-light-responsive kaolin-supported Ag @ AgBr composites and their enhanced photocatalytic properties, Appl. Clay Sci. 175 (2019) 76–85. https://doi.org/10.1016/j.clay.2019.04.003.

[22] O.A. Oyewo, A. Adeniyi, B.B. Sithole, M.S. Onyango, Sawdust-Based Cellulose Nanocrystals Incorporated with ZnO Nanoparticles as E ffi cient Adsorption Media in the Removal of Methylene Blue Dye, ACSOMEGA. (2020). https://doi.org/10.1021/acsomega.0c01924.

[23] R.P. Cavalcante, R.F. Dantas, B. Bayarri, O. González, J. Giménez, S. Esplugas, A. Machulek, Photocatalytic mechanism of metoprolol oxidation by photocatalysts TiO2 and TiO2 doped with 5% B: Primary active species and intermediates, Appl. Catal. B Environ. 194 (2016) 111–122. https://doi.org/10.1016/J.APCATB.2016.04.054.

[24] Y. Zhao, Z. Cao, A.A. Zuh, Y. Jia, Q. Wang, H. Cheng, Synthesis of bismuth oxyiodide/kaolinite composite with enhanced photocatalytic activity, J. Phys. Chem. Solids. 161 (2022) 110424. https://doi.org/10.1016/j.jpcs.2021.110424.

[25] X. Tan, X. Li, T. Yu, Y. Zhao, Preparation and photocatalytic activity of BiOBr/TiO2 heterojunction nanocomposites, Trans. Tianjin Univ. 22 (2016) 211–217. https://doi.org/10.1007/s12209-016-2778-8.

[26] R. Kumar, P. Raizada, A.A.P. Khan, V.H. Nguyen, Q. Van Le, S. Ghotekar, R. Selvasembian, V. Gandhi, A. Singh, P. Singh, Recent progress in emerging BiPO4-based photocatalysts: Synthesis, properties, modification strategies, and photocatalytic applications, J. Mater. Sci. Technol. 108 (2022) 208–225. https://doi.org/10.1016/j.jmst.2021.08.053.

[27] X. Liu, S. Gu, Y. Zhao, G. Zhou, W. Li, BiVO4, Bi2WO6 and Bi2MoO6 photocatalysis: A brief review, J. Mater. Sci. Technol. 56 (2020) 45–68. https://doi.org/10.1016/j.jmst.2020.04.023.

[28] S. Irfan, Z. Zhuanghao, F. Li, Y.X. Chen, G.X. Liang, J.T. Luo, F. Ping, Critical review: Bismuth ferrite as an emerging visible light active nanostructured photocatalyst, J. Mater. Res. Technol. 8 (2019) 6375–6389. https://doi.org/10.1016/j.jmrt.2019.10.004.

[29] Z. Chen, X. Jiang, C. Zhu, C. Shi, Chromium-modified Bi4Ti3O12 photocatalyst: Application for hydrogen evolution and pollutant degradation, Appl. Catal. B Environ. 199 (2016) 241–251. https://doi.org/10.1016/j.apcatb.2016.06.036.

[30] G.Q. Zhao, J. Hu, J. Zou, X. Long, F.P. Jiao, Modulation of BiOBr-based photocatalysts for energy and environmental application: A critical review, J. Environ. Chem. Eng. 10 (2022) 107226. https://doi.org/10.1016/j.jece.2022.107226.

[31] S.S. Imam, R. Adnan, N.H. Mohd Kaus, The photocatalytic potential of BiOBr for wastewater treatment: A mini-review, J. Environ. Chem. Eng. 9 (2021) 105404. https://doi.org/10.1016/j.jece.2021.105404.

[32] X. Chang, M.A. Gondal, A.A. Al-Saadi, M.A. Ali, H. Shen, Q. Zhou, J. Zhang, M. Du, Y. Liu, G. Ji, Photodegradation of Rhodamine B over unexcited semiconductor compounds of BiOCl and BiOBr, J. Colloid Interface Sci. 377 (2012) 291–298. https://doi.org/10.1016/j.jcis.2012.03.021.

[33] L. Meng, Y. Qu, L. Jing, Recent advances in BiOBr-based photocatalysts for environmental remediation, Chinese Chem. Lett. 32 (2021) 3265–3276. https://doi.org/10.1016/j.cclet.2021.03.083.

[34] H. Yang, Q. Zhang, Y. Chen, Y. Huang, F. Yang, Z. Lu, Ultrasonic-microwave synthesis of ZnO/BiOBr functionalized cotton fabrics with antibacterial and photocatalytic properties, Carbohydr. Polym. 201 (2018) 162–171. https://doi.org/10.1016/j.carbpol.2018.08.068.

[35] Y. Tian, J. Zhang, W. Wang, J. Liu, X. Zheng, J. Li, X. Guan, Facile assembly and excellent elimination behavior of porous BiOBr-g-C3N4 heterojunctions for organic pollutants, Environ. Res. 209 (2022) 112889. https://doi.org/10.1016/j.envres.2022.112889.

[36] R. Haounati, H. Ighnih, H. Ouachtak, R.E. Malekshah, N. Hafid, A. Jada, A. Ait, Z-Scheme g-C3N4/Fe3O4/Ag3PO4@Sep magnetic nanocomposites as heterojunction photocatalysts for green malachite degradation and Dynamic molecular studies, Colloids Surfaces A Physicochem. Eng. Asp. (2023) 131509. https://doi.org/10.1016/j.colsurfa.2023.131509.

[37] C. Xu, H. Wu, F.L. Gu, Efficient adsorption and photocatalytic degradation of Rhodamine B under visible light irradiation over BiOBr/montmorillonite composites, J. Hazard. Mater. 275 (2014) 185–192. https://doi.org/10.1016/j.jhazmat.2014.04.064.

[38] Y. Wang, Q. Yang, X. Wang, J. Yang, Y. Dai, Y. He, W. Chen, W. Zhang, Photocatalytic degradation of rhodamin B and diclofenac sodium on hollow hierarchical microspheres of BiOBr modified with sepiolite and polyvinyl pyrrolidone (PVP), Mater. Sci. Eng. B. 244 (2019) 12–22. https://doi.org/10.1016/j.mseb.2019.04.005.

[39] Z. Cao, Q. Wang, H. Cheng, Recent advances in kaolinite-based material for photocatalysts, Chinese Chem. Lett. (2021). https://doi.org/10.1016/j.cclet.2021.01.009.

[40] H. Ighnih, R. Haounati, R. Eshaghi, H. Ouachtak, A. Jada, A. Ait, Photocatalytic degradation of RhB dye using hybrid nanocomposite BiOCl@Kaol under sunlight irradiation, J. Water Process Eng. 54 (2023) 103925. https://doi.org/10.1016/j.jwpe.2023.103925.

[41] B. Li, S. Liu, J. Guo, L. Zhang, Interaction between low rank coal and kaolinite particles: A DFT simulation, Appl. Surf. Sci. 456 (2018) 215–220. https://doi.org/10.1016/J.APSUSC.2018.06.121.

[42] X. Fei, L. Zhang, J. Yu, B. Zhu, DFT Study on Regulating the Electronic Structure and CO 2 Reduction Reaction in BiOBr / Heterojunctions, Front. Nanotechnol. 3 (2021) 1–10. https://doi.org/10.3389/fnano.2021.698351.

[43] I. Salahshoori, A. Babapoor, A. Seyfaee, Elevated performance of the neat , hybrid and composite membranes by the addition of nanoparticles (ZIF-67): A molecular dynamics study, Springer Berlin Heidelberg, 2022. https://doi.org/10.1007/s00289-021-03673-2.

[44] M.C. Dlamini, M.L. Dlamini, P. Mente, B. Tlhaole, R. Erasmus, M.S. Maubane-Nkadimeng, J.A. Moma, Photocatalytic abatement of phenol on amorphous TiO2-BiOBr-bentonite heterostructures under visible light irradiation, J. Ind. Eng. Chem. 111 (2022) 419–436. https://doi.org/10.1016/j.jiec.2022.04.023.

[45] C. Chuaicham, K. Sekar, V. Balakumar, J. Uchida, T. Katsurao, H. Sakabe, B. Ohtani, K. Sasaki, Efficient photocatalytic degradation of emerging ciprofloxacin under visible light irradiation using BiOBr/carbon quantum dot/saponite composite, Environ. Res. 212 (2022) 113635. https://doi.org/10.1016/j.envres.2022.113635.

[46] Z. Sun, G. Yao, X. Zhang, S. Zheng, R.L. Frost, Enhanced visible-light photocatalytic activity of kaolinite / g-C 3 N 4 composite synthesized via mechanochemical treatment, Appl. Clay Sci. 129 (2016) 7–14. https://doi.org/10.1016/j.clay.2016.04.003.

[47] M.R. Abukhadra, A. Alhammadi, A.M. El-sherbeeny, A. Salam, M.A. El-meligy, E. Mahrous, M. Luqman, Enhancing the removal of organic and inorganic selenium ions using an exfoliated kaolinite / cellulose fibres nanocomposite, Carbohydr. Polym. 252 (2021) 117163. https://doi.org/10.1016/j.carbpol.2020.117163.

[48] S. Wang, H. Yin, J. Ding, H. Chen, L. Wang, Y. Zhou, K. Liu, J. Wang, One-pot preparation of novel Bi/BiOBr/Bi2O2CO3 heterojunction for pollutant degradation under visible light: Catalyst generation insights, reaction mechanism, degradation pathways, and toxicological effects, Surfaces and Interfaces. 37 (2023) 102642. https://doi.org/10.1016/j.surfin.2023.102642.

[49] C. Zhao, Y. Liang, W. Li, X. Chen, Y. Tian, D. Yin, Q. Zhang, 3D BiOBr/BiOCl

heterostructure microspheres with enhanced photocatalytic activity, J. Mater. Sci. Mater. Electron. 31 (2020) 1868–1878. https://doi.org/10.1007/s10854-019-02706-x.

[50] J. Wang, H. Li, X. Yan, C. Qian, Y. Xing, S. Yang, Z. Kang, J. Han, W. Gu, H. Yang, F. Xiao, Synergistic enhancement of the visible-light photocatalytic activity of hierarchical 3D BiOClxBr1-x/graphene oxide heterojunctions for formaldehyde degradation at room temperature, J. Alloys Compd. 795 (2019) 120–133. https://doi.org/10.1016/j.jallcom.2019.04.176.

[51] G. Zhang, Z. Sun, X. Hu, A. Song, S. Zheng, Synthesis of BiOCl/TiO2–zeolite composite with enhanced visible light photoactivity, J. Taiwan Inst. Chem. Eng. 81 (2017) 435–444. https://doi.org/10.1016/j.jtice.2017.09.030.

[52] Z. Yang, Q. Lin, G. Zeng, S. Zhao, G. Yan, M.B.M.Y. Ang, Y.H. Chiao, S. Pu, Ternary hetero-structured BiOBr/Bi2MoO6@MXene composite membrane: Construction and enhanced removal of antibiotics and dyes from water, J. Memb. Sci. 669 (2023) 121329. https://doi.org/10.1016/j.memsci.2022.121329.

[53] Q. Lin, G. Zeng, G. Yan, J. Luo, X. Cheng, Z. Zhao, H. Li, Self-cleaning photocatalytic MXene composite membrane for synergistically enhanced water treatment: Oil/water separation and dyes removal, Chem. Eng. J. 427 (2022) 131668. https://doi.org/10.1016/j.cej.2021.131668.

[54] R. Pelalak, R. Soltani, Z. Heidari, R.E. Malekshah, M. Aallaei, A. Marjani, M. Rezakazemi, T.A. Kurniawan, S. Shirazian, Molecular dynamics simulation of novel diamino-functionalized hollow mesosilica spheres for adsorption of dyes from synthetic wastewater, J. Mol. Liq. 322 (2021). https://doi.org/10.1016/j.molliq.2020.114812.

[55] J. Chen, F. fei Min, L. yun Liu, C. fu Liu, Mechanism research on surface hydration of kaolinite, insights from DFT and MD simulations, Appl. Surf. Sci. 476 (2019) 6–15. https://doi.org/10.1016/j.apsusc.2019.01.081.

[56] I. Salahshoori, M. Namayandeh Jorabchi, K. Valizadeh, A. Yazdanbakhsh, A. Bateni, S. Wohlrab, A deep insight of solubility behavior, mechanical quantum, thermodynamic, and mechanical properties of Pebax-1657 polymer blends with various types of vinyl polymers: A mechanical quantum and molecular dynamics simulation study, J. Mol. Liq. 363 (2022) 119793. https://doi.org/10.1016/j.molliq.2022.119793.

[57] T. Xiong, H. Wang, Y. Zhou, Y. Sun, W. Cen, g-C3N4for enhanced visible light photocatalytic, Nanopart Res. (2018) 8066–8074.

[58] M. He, W. Li, J. Xia, L. Xu, J. Di, H. Xu, S. Yin, H. Li, M. Li, The enhanced visible light photocatalytic activity of yttrium-doped BiOBr synthesized via a reactable ionic liquid, Appl. Surf. Sci. 331 (2015) 170–178. https://doi.org/10.1016/j.apsusc.2014.12.141.

[59] C. Wu, C. Zhou, Y. Chen, Z. Peng, J. Yang, Y. Zhang, Simple Fabrication of Visible Light-Responsive Bi-BiOBr/BiPO4Heterostructure with Enhanced Photocatalytic Activity, J. Nanomater. 2021 (2021). https://doi.org/10.1155/2021/4835596.

[60] R. Haounati, H. Ighnih, R.E. Malekshah, S. Alahiane, F. Alakhras, E. Alabbad, H. Alghamdi, H. Ouachtak, A.A. Addi, A. Jada, Exploring ZnO/Montmorillonite photocatalysts for the removal of hazardous RhB Dye: A combined study using molecular dynamics simulations and experiments, Mater. Today Commun. 35 (2023) 105915. https://doi.org/10.1016/J.MTCOMM.2023.105915.

[61] E. Hass Caetano Lacerda, F.C. Monteiro, J.R. Kloss, S.T. Fujiwara, Bentonite clay modified with Nb2O5: An efficient and reused photocatalyst for the degradation of reactive textile dye, J. Photochem. Photobiol. A Chem. 388 (2020). https://doi.org/10.1016/j.jphotochem.2019.112084.

[62] A.O.C. Andrade, L.H. da S. Lacerda, M.M. Lage Júnior, S.K. Sharma, M.E.H. Maia da Costa, O.C. Alves, E.C.S. Santos, C.C. dos Santos, A.S. de Menezes, M.A. San-Miguel, F.M. Filho, E. Longo, M.A.P. Almeida, Enhanced photocatalytic activity of BiOBr/ZnWO4 heterojunction: A combined experimental and DFT-based theoretical approach, Opt. Mater. (Amst). 138 (2023) 113701. https://doi.org/10.1016/j.optmat.2023.113701.

[63] M. Zhang, H. fei Yin, J. cheng Yao, M. Arif, B. Qiu, P. fei Li, X. heng Liu, All-solid-state Z-scheme BiOX(Cl, Br)-Au-CdS heterostructure: Photocatalytic activity and degradation pathway, Colloids Surfaces A Physicochem. Eng. Asp. 602 (2020) 124778. https://doi.org/10.1016/j.colsurfa.2020.124778.